Journal of Medicinal Chemistry

Article

Profiling of flavonol derivatives for the development of anti-trypanosomatidic drugs

Chiara Borsari, Rosaria Luciani, Cecilia Pozzi, Ina Pöhner, Stefan Henrich, Matteo Trande, Anabela Cordeiro-da-Silva, Nuno Santarém, Catarina Baptista, Annalisa Tait, Flavio Di Pisa, Lucia Dello Iacono, Giacomo Landi, Sheraz Gul, Markus Wolf, Maria Kuzikov, Bernhard Ellinger, Jeanette Reinshagen, Gesa Witt, Philip Gribbon, Manfred Kohler, Oliver Keminer, Birte Behrens, Luca Costantino, Paloma Tejera Nevado, Eugenia Bifeld, Julia Eick, Joachim Clos, Juan Torrado, María Dolores Jiménez-Antón, Maria Jesùs Corral, José Maria Alunda, Federica Pellati, Rebecca C Wade, Stefania Ferrari, Stefano Mangani, and Maria Paola Costi

J. Med. Chem., **Just Accepted Manuscript** • DOI: 10.1021/acs.jmedchem.6b00698 • Publication Date (Web): 14 Jul 2016

ACS Publications

Journal of Medicinal Chemistry is published by the American Chemical Society. 1155 Sixteenth Street N.W., Washington, DC 20036

	Pharmacy Jiménez-Antón, María; Dpto Farmacia y Tecnología Farmacéutica, Facultad de Farmacia, Complutense University of Madrid, Plaza Ramón y Cajal, Pharmacy Corral, Maria; Dpto Farmacia y Tecnología Farmacéutica, Facultad de Farmacia, Complutense University of Madrid, Plaza Ramón y Cajal, Pharmacy Alunda, José; Dpto Farmacia y Tecnología Farmacéutica, Facultad de Farmacia, Complutense University of Madrid, Plaza Ramón y Cajal, Pharmacy Pellati, Federica; University of Modena and Reggio Emilia, Department of Life Sciences Wade, Rebecca; HITS gGmbH, Molecular and Cellular Modeling Ferrari, Stefania; Università degli Studi di Modena e Reggio Emilia, Dipartimento di Scienze della Vita Mangani, Stefano; University of Siena, Biotechnology Chemistry and Pharmacy Costi, Maria Paola; Universita Di Modena e Reggio Emilia, Dipartimento Di Scienze della Vita

Profiling of flavonol derivatives for the development of anti-trypanosomatidic drugs

Borsari, Chiara[1^]; Luciani,Rosaria[1^]; Pozzi, Cecilia[2^]; Poehner, Ina[3^]; Henrich, Stefan[3]; Matteo, Trande[1], Cordeiro-da-Silva, Anabela[4]; Santarem, Nuno[4]; Baptista, Catarina[4]; Tait, Annalisa[1]; Di Pisa, Flavio[2]; Dello Iacono Lucia[2], Landi, Giacomo[2]; Gul, Sheraz[5]; Wolf, Markus[5]; Kuzikov, Maria[5]; Ellinger, Bernhard[5]; Reinshagen, Jeanette[5]; Witt, Gesa[5]; Gribbon, Philip[5]; Manfred Kohler[5]; Keminer, Oliver[5]; Behrens,Birte[5]; Costantino, Luca[1]; Tejera Nevado, Paloma[9]; Bifeld, Eugenia[9]; Eick, Julia[9]; Clos, Joachim[9]; Torrado, Juan [6]; Jiménez-Antón, María D.[6,10]; Corral, María J. [6,10]; Alunda, José M[a6,10]; Federica, Pellati[1]; Wade, Rebecca C.[3,7,8]; Ferrari, Stefania[1*]; Mangani, Stefano[2*]; Costi, Maria Paola[1*].

[1]*Department of Life Sciences, University of Modena and Reggio Emilia, Italy, Via G. Campi 103, 41125 Modena, Italy.*

[2]*Department of Biotechnology, Chemistry and Pharmacy,University of Siena, Italy, Via Aldo Moro 2, 53100 Siena, Italy.*

[3]*Molecular and Cellular Modeling Group, Heidelberg Institute for Theoretical Studies, 69118 Heidelberg, Germany.*

[4]*Institute for Molecular and Cell Biology, Porto, Portugal.*

[5]*Fraunhofer Institute for Molecular Biology and Applied Ecology ScreeningPort, Schnackenburgallee 114 D-22525, Hamburg, Germany.*

[6]*Complutense University of Madrid, 28040 Madrid, Spain.*

[7]*Center for Molecular Biology (ZMBH), DKFZ-ZMBH Alliance, Heidelberg University, 69120 Heidelberg, Germany.*

[8]*Interdisciplinary Center for Scientific Computing (IWR), Heidelberg University,69120 Heidelberg, Germany.*

[9]*Bernhard Nocht Institute for Tropical Medicine, D-20359 Hamburg, Germany.*

[10]*Instituto de Investigación Hospital 12 de Octubre, 28041 Madrid, Spain.*

KEYWORDS: Neglected diseases, flavonols, antiparasitic activity, pteridine reductase 1.

Abstract

Flavonoids represent a potential source of new anti-trypanosomatidic leads. Starting from a library of natural products, we combined target-based screening on pteridine reductase 1 with phenotypic screening on *Trypanosoma brucei*, for hit identification. Flavonols were identified as hits and a library of 16 derivatives was synthesized. Twelve compounds showed EC_{50} values against *T. brucei* below 10 μM. Four X-ray crystal structures and docking studies explained the observed structure-activity relationships. Compound **2** (3,6-dihydroxy-2-(3-hydroxyphenyl)-4H-chromen-4-one) was selected for pharmacokinetic studies. Encapsulation of compound **2** in PLGA nanoparticles or cyclodextrins resulted in lower *in-vitro* toxicity when compared to the free compound. Combination studies with methotrexate revealed that compound **13** (3-hydroxy-6-methoxy-2-(4-methoxyphenyl)-4H-chromen-4-one) has the highest synergistic effect at concentration of 1.3μM, 11.7 folds dose reduction index and no toxicity towards host cells. Our results provide the basis for further chemical modifications aimed at identifying novel antitrypanosomatidic agents showing higher potency towards PTR1 and increased metabolic stability.

Introduction

Protozoan parasites of the Trypanosomatidae family are the etiological agents of several significant neglected tropical diseases including Human African Trypanosomiasis (HAT), Chagas' disease and Leishmaniasis, which collectively affect nearly 10 million people worldwide. HAT is caused by the bloodstream form of *Trypanosoma brucei.*[1] *Leishmania spp*. infect macrophages and cause a wide spectrum of symptoms ranging from cutaneous lesions to potentially fatal visceral infections.[2] *Trypanosoma cruzi*, the etiological agent of Chagas disease, is an obligate intracellular parasite that invades different internal organs. Since effective vaccines are lacking, the control of these diseases is based on vector control and chemotherapy. However, the drugs currently available are characterized by high toxicity, limited efficacy and require a long period of treatment. The first line drugs have been used for over half a century and their efficacy is compromised by widespread resistance.[3-5] Therefore, there is an urgent requirement for new, safe and effective drugs. The drug discovery process against these parasites is hampered by the intrinsic biology of these organisms that can include intracellular stages or central nervous system involvement.[6]

Although there are very few validated drug targets for Leishmaniasis and HAT, a target-based approach is extensively used in the drug discovery process for neglected tropical diseases.[7] The folate pathway is an established target for the treatment of bacterial infections and some parasitic diseases, such as malaria.[8] Drugs targeting folate-dependent enzymes represent useful candidates against trypanosomatidic infections and key enzymes of the folate metabolism are thymidylate synthase (TS) and dihydrofolate reductase (DHFR), which is the target of the antifolate drugs methotrexate (MTX), pyrimethamine (PYR) and trimethoprim (TMP). However, the activity of classical inhibitors of DHFR against *Leishmania* and *Trypanosoma* is reduced because of pteridine reductase 1 (PTR1).[9] PTR1 is responsible for the salvage of pterins in parasitic trypanosomatids and has overlapping activity with DHFR, providing a metabolic bypass to alleviate DHFR inhibition.[10-12] Under physiological conditions, PTR1 is responsible for only 10% of the reduction of folic acid required by

the cell, but when classic anti-folate drugs inhibit DHFR, the gene encoding the NADPH-dependent PTR1 is up regulated and PTR1 provides the reduced folates necessary for parasite survival.[13] Therefore, PTR1 is considered a promising target for the development of improved therapies. This protein is considered a validated target in *T. brucei*, even though a correlation between inhibition of *T. brucei* PTR1 (*Tb*PTR1) and inhibition of parasite growth has not been demonstrated yet. The combination with MTX, a DHFR inhibitor, has been shown to improve the efficacy and the potency of PTR1 inhibitors.[14,15]

In the drug discovery process, natural compounds represent a potential source of newleads.[16-19] Different natural compounds from plants including flavonoids have shown anti-trypanosomatidic activity.[20,21] Although flavonoids have been found to inhibit polyamine biosynthesis, the mechanism of action has not been fully elucidated.[21-24] Flavonoids exert pleiotropic effects and different targets have been suggested to explain at least part of their anti-parasitic activity.[25-27] Flavonoids have been proposed as PTR1 inhibitors only *in-silico*.[28] Although some flavonoids are very effective *in-vitro*, they lack notable *in-vivo* activity due to their low bioavailability.[22] However, an efficient drug delivery strategy together with a clear definition of their molecular targets could lead to the exploitation of the anti-parasitic potential of these natural products.[22]

The purpose of the present study was to identify new PTR1 inhibitors showing anti-trypanosomal (*T. brucei, T. cruzi*) and anti-leishmanial (*Leishmania infantum*) activity by screening a library of natural products and then by using a medicinal chemistry approach to design, synthesize and biologically evaluate a new library. Assessment of early ADME and toxicity properties provided selection criteria for further studies. MTX has previously been combined with PTR1 inhibitors to achieve synergistic/additive effects on *T. brucei*.[14] In our study, we evaluated the antiparasitic activity of the compounds both alone and in combination with MTX. Pharmacokinetic studies using BALB/c mice showed that one of our compounds (compound **2**) was characterized by a short half-life and therefore

it was loaded in Poly(lactic-co-glycolicacid) (PLGA) nanoparticles and solubilized with cyclodextrins aiming to increase the its stability and bioavailability.

Results and discussion

On-target screening of a natural product library and hit identification

To identify potential new drugs for treating parasitic diseases, we investigated a library of natural products. Starting from a library of 98 compounds, a computational docking analysis against *Tb*PTR1 together with consideration of structural diversity allowed the restriction of the library to 38 compounds that were tested for PTR1 inhibition. These 38 phytochemicals (**NP-1** – **NP-38**) consisting of 12 phenolic acids, 5 flavanones, 9 flavones, 6 flavonols, 2 catechins, 2 triterpenes and 2 anthraquinones, were investigated for *in-vitro* inhibition of *Tb*PTR1 and for growth inhibition of *T. brucei*. Due to their ability to bind similar folate-related metabolites, PTR1 inhibitors can also interact with other folate-dependent enzymes such as TS and DHFR both from parasite and human cells. Both human enzymes can be considered potential off-targets for PTR1 inhibitors, therefore all the compounds were assessed for their selectivity towards the human TS and human DHFR. The data obtained are depicted in Figure 1. All chemical structures and IC_{50} values are reported in Table S1 of the Supporting Information.

With the exception of quercetin dehydrate (**NP-30**), all flavon-3-ol type aglycones showed a significant *Tb*PTR1 inhibition, with 3-hydroxyflavone (**NP-27**, IC_{50} = 12.8 μM) and isorhamnetin (**NP-31**, IC_{50} = 13.9 μM) being the most potent; whereas the glycosylated flavonoid (**NP-32**) did not inhibit *Tb*PTR1. Most phenolic acids showed no inhibitory activity towards *Tb*PTR1, highlighting the importance of a condensed ring (chromen-4-one) for protein inhibition. The presence of two rings, one aromatic and the other one aliphatic (**NP-8**) or both aromatic (**NP-10**), slightly increased the inhibitory activity with respect to the other phenolic acid derivatives.

The simplest flavonol (**NP-27**, IC_{50} = 12.8 μM) was 10 times more potent than the corresponding flavone (**NP-18**, IC_{50} = 120.8 μM). This implies the importance of OH at position R3. Moreover, isorhamnetin (**NP-31**, IC_{50} = 13.9 μM) was over 35 times more active against *Tb*PTR1 than the corresponding flavone (chrysoeriol, **NP-25**, IC_{50}>490μM). The insertion of a hydroxyl group at position R5 led to a decrease in the inhibitory activity. Indeed, the simplest flavone (**NP-18**, IC_{50} = 120.8 μM) is more than 20-fold more active than primuletin (**NP-19**, IC_{50}>2450 μM), which has a hydroxyl group at position 5. On target screening of the NP series indicates that flavonols are the most promising compounds, with **NP-31** being the most active and selective hit (Selectivity Index – SI hTS/*Tb*PTR1 >35; SI hDHFR/*Tb*PTR1 = 36). Nevertheless, a clear structure-activity relationship (SAR) could not be established from this dataset and we could not reliably determine how the number and the pattern of hydroxyl/methoxy substituents influenced the activity.

The 38 compounds were also assessed for their inhibitory activity against *T. brucei* parasite (Figure 1, Table S1). With the exception of **NP-9**, **NP-10**, **NP-22**, and **NP-35**, all the natural flavonoids screened showed anti-trypanosomal activity with IC_{50} lower than 30 μM. Figure 1 shows that there is no direct correlation between the anti-trypanosomal activity of the NP compounds and their PTR1 inhibition effect.

X-ray crystallographic studies of the natural products

To understand the flavonoid interactions into the protein binding site, the 18 compounds showing IC_{50} lower than 150 μM (compounds **NP-8**, **NP-10**, **NP-12**, **NP-13**, **NP-18**, **NP-21**, **NP-22**, **NP-23**, **NP-24**, **NP-26**, **NP-27**, **NP-28**, **NP-29**, **NP-31**, **NP-35** and **NP-36**; Figure 1) were selected for structural analysis. We obtained crystal structures of the *Tb*PTR1-NADPH/$NADP^+$ complexes for two moderately active natural products (**NP-29** (datiscetin) IC_{50} *Tb*PTR1= 76.9 μM and **NP-13** (hesperetin) IC_{50} = 104.2 μM) only. These compounds show inhibitory activity against *Tb*PTR1 and selectivity against at least one of the human proteins (TS and DHFR; Figure 1). Statistics for data collection and refinement are reported in Tables S2 and S3 of the Supporting Information. In both

cases, the crystal asymmetric unit contains the functional unit of the enzyme, the *Tb*PTR1 tetramer. The tertiary structure of the *Tb*PTR1 subunits is typical of the short-chain dehydrogenases/reductases (SDR) superfamily and shows a single α/β domain consisting of a seven-stranded parallel β-sheet sandwiched between two sets of α-helices.[29] The *Tb*PTR1 active site is mainly formed by a single chain, with one end blocked by the C-terminus of the partner subunit. In this L-shaped depression, the cofactor binds in an extended conformation entrapped by a network of highly conserved hydrogen bonds.[29] The substrate-binding loop (residues 207-215) interacts with both the cofactor and the substrate. Two surface-exposed parts of the sequence, residues 104 to 112 and 143 to 151, are usually poorly visible in *Tb*PTR1 crystal structures, and they were not included in our models. The overall structure of each subunit of the *Tb*PTR1 complexes is the same as indicated by the small root mean square deviations (RMSDs) after Cα superimposition of the four subunits in each tetramer (0.16-0.26Å for **NP-13** and 0.11 – 0.41 Å for **NP-29**). The binding of the cofactor is essential to create both the catalytic site and the substrate-binding pocket, indicating an ordered sequential reaction mechanism with NADPH binding before the substrate.[30] The pterin moiety of substrates and of pterin-like inhibitors binds in a π-sandwich between the nicotinamide ring of NADPH/$NADP^+$ and the aromatic side chain of Phe97.[31] Pterin also interacts with the NADPH/$NADP^+$β-phosphate, and this interaction is strongly conserved in pterin-like inhibitors.[31]

***Tb*PTR1-NADPH/$NADP^+$-NP-29**. The chromen-4-one core of **NP-29** binds in the biopterin binding pocket as described above. The ligand is supported by a network of H-bonds involving the cofactor and the surrounding residues in the active site cavity (see Figure 2A). The hydroxyl group at position 7 on the chromen-4-one of **NP-29** (the **NP-29** atom numbering is given in the inset in Figure 2A) donates a H-bond to the NADPH/$NADP^+$β-phosphate and accepts a H-bond from an amino group on Arg14. The hydroxyl group at position 5 accepts a H-bond from NADPH/$NADP^+$ ribose OH2' and donates a H-bond to the hydroxyl group of Tyr174 which in turn donates a H-bond to the inhibitor carbonyl oxygen at position 4. Furthermore, the carbonyl oxygen and the hydroxyl group at position 3 of **NP-29** are both H-bonded to a water molecule linked by a further H-bond to the side chain of

Asp161. An additional water molecule, which is highly conserved throughout all *Tb*PTR1 structures, mediates the interaction between the position 3 hydroxyl group of **NP-29** and the backbone carbonyl oxygen of Gly205 (not shown). The o-phenol moiety of **NP-29** is located in a hydrophobic pocket of the *Tb*PTR1 active site cavity, surrounded by the side chains of Val206, Leu209, Pro210, Met213 and Trp221. The 2' hydroxyl group on this ring is close (~ 4 Å) to the carbonyl oxygen of Gly205 and forms an intramolecular H-bond (2.4 Å) with the hydroxyl group at the 3 position on the chromen-4-one moiety.

***Tb*PTR1-NADPH/NADP$^+$-NP-13**. The chromen-4-one core of **NP-13** also binds in the biopterin binding pocket, but it is rotated by about 180° with respect to its orientation in the *Tb*PTR1-**NP-29** complex (Figure 2B). The ether oxygen at position 1 on the chromen-4-one moiety of **NP-13** points towards the side chains of Asp161 and Tyr174. The hydroxyl group at position 7 of the **NP-13** chromen-4-one is within H-bonding distance of the NADPH/NADP$^+$ ribose OH2' and the side chain of Ser95. The **NP-13** hydroxyl group at position 5 accepts a H-bond from an amino group of Arg14 and donates a H-bond to the backbone carbonyl oxygen of Leu208. The o-methoxy-phenol (o-guaiacol) ring in position 2 on the chromen-4-onemakes a T-shaped stacking interaction with the aromatic side chain of Trp221. Furthermore, the 3' phenolic moiety is within H-bonding distance of the Asp161 side chain and forms two water-mediated interactions with the backbone nitrogen of Cys168 and the amide nitrogen of Asn175 (not shown). The methoxy oxygen at the 4' position interacts with the sulfur of the modified Cys168 (S-oxy-cysteine), whereas the terminal methyl makes van der Waals contacts with the side chains of Trp221 and His267 of the partner subunit.

In summary, structural comparison of the two *Tb*PTR1 complexes reveals two opposite orientations of the natural flavonoid inhibitors **NP-13** and **NP-29** in the biopterin binding pocket in which the chromen-4-one substituents interact with different residues surrounding the cavity. A double binding mode was previously observed for pteridine-like inhibitors and MTX.[15]

Flavonoid library design and synthesis

The crystal structures showed that flavonoids occupy the biopterin binding site of *Tb*PTR1, suggesting that the flavonol moiety could provide a new scaffold for the development of PTR1 inhibitors. The flavonoids selected as starting points for the development of compounds to treat trypanosomatidic diseases are depicted in Table 1. Even though the two crystal structures showed that the hydroxyl group at position 5 could establish H-bonds with the protein and the cofactor, the inhibitory data on natural flavonoids (Figure 1) suggested that a hydroxyl group in this position leads to a decrease in the inhibitory activity against *Tb*PTR1. Therefore, we decided to synthesize compounds with hydroxyl substituents at positions 6 or 7 of the chromenone A-ring since, according to the crystal structures, these should be able to establish H-bonds with the NADPH/$NADP^+$ ribose and the side chain of Ser95 or with the NADPH/$NADP^+$β-phosphate and Arg14 (Figure 3). Moreover, we performed modifications at positions 3', 4' and 5' on ring B to explore the SAR. As shown in Figure 3, hydroxyl groups in positions 3', 4'and 5' could form a H-bonding interaction with the Asp161 side chain and two water-mediated interactions with the backbone nitrogen of Cys168 and the amide nitrogen of Asn175. Many natural products have both hydroxyl and methoxy groups, thus we synthesized and biologically evaluated eight hydroxylated (**1-8**) and eight methoxylated (**9-16**) compounds aiming to investigate how the number and the pattern of hydroxyl/methoxy substituents influenced the activity.

The synthesis of compounds **1-16** is depicted in Scheme 1. All the compounds have been already reported in literature, but, as far as we know, they have never been proposed as PTR1 inhibitors. The intermediate chalcones (**17-24**) were synthesized by Claisen-Schmidt condensation using substituted acetophenones and benzaldehydes in the presence of NaOH as the base in ethanol. The reaction was carried out as previously reported in literature for similar compounds.[26] Afterwards, the chalcones (**17-24**) were converted into the corresponding methoxylated flavonols (**9-16**), using the Flynn-Algar-Oyamada method for epoxidation and subsequent intramolecular cyclization of the open-chain structure.[25] The reaction was performed with hydrogen peroxide in aqueous base (1 M NaOH). Cleavage of methoxy protecting groups with boron tribromide gave the hydroxylated flavonols **1-8** in

high yield. All synthesized compounds were characterized by ^{1}H-NMR, ^{13}C-NMR and mass analysis. The obtained NMR and mass data are reported in the Supporting Information (pag. 33-37) and were compared with those available in literature.

Target compound profile

In our study a panel of assays was performed and activity/toxicity data were considered during the hit selection/prioritization.[32] Together with the potency data (measured as IC_{50} i.e. the compound concentration producing 50% reduction of targeted enzyme activity and parasite cell growth), we considered the selectivity index (IC_{50} towards the parasite compared with compound cytotoxicity IC_{50} to host cells) and early-toxicity properties. We have assessed the entire profile of the sixteen synthesized compounds and the whole data panel has been evaluated before selecting compounds for pharmacokinetic studies.

Testing of synthetic flavonols against PTR1 enzymes

All flavonols were investigated for their activity towards *T. brucei* (*Tb*PTR1) and *L. major* PTR1 (*Lm*PTR1). The results are shown in Figure 4 and Table S4 of the Supporting Information. All hydroxylated compounds except compound **5** showed significant inhibitory activity against *Lm*PTR1 and *Tb*PTR1 at 50 μM concentration, with compound **2** being the most potent. Methylation resulted in almost complete loss of inhibitory activity. The most noteworthy examples are represented by two pairs: compounds **10** and **2** (4 % and 96 % inhibition of *Tb*PTR1 at 50 μM, respectively) and compounds **12** and **4** (no inhibition of *Tb*PTR1 at 50 μM and 85 % inhibition at 50 μM, respectively). The introduction of a hydroxyl group on ring A in compound **2** led to a significant increase of almost 3-fold in the inhibitory potency against both enzymes with respect to compound **1**, which bears an unsubstituted ring (34 % inhibition of *Tb*PTR1 at 50 μM). In order to explain a complete SAR, X-ray crystallographic studies and docking analyses were carried out. The compounds were evaluated towards also towards TcPTR2 and none of the compound significantly inhibited TcPTR2 activity (data not shown).

Crystal structures of synthetic flavonoid-*Tb*PTR1 complexes

Compounds **2** and **7**, which show inhibitory activity against *Tb*PTR1, were submitted to X-ray crystallographic characterization aimed at comparing their binding poses in the PTR1 active site with those of the natural flavonoids and thus gaining further information for compound optimization.

***Tb*PTR1-NADPH/NADP$^+$-2.** The structure of *Tb*PTR1 in complex with NADPH/NADP$^+$ and compound **2** was determined at 1.38Å resolution. Ligand placement and key interactions within the active site cavity are reported in Figure 2C. Compound **2**, like **NP-13** and **NP-29**, binds in the substrate binding pocket, with the chromen-4-one in a π-sandwich interaction between the nicotinamide ring of NADPH/NADP$^+$ and the aromatic side chain of Phe97. The chromen-4-one core of compound **2** adopts the binding mode observed for **NP-13**, with the oxygen atom at position 1 directed towards the side chain of Asp161. The R6 hydroxyl group on the chromen-4-one is within H-bonding distance of the hydroxyl group of Ser95 and the NADPH/NADP$^+$β-phosphate oxygen. The carbonyl oxygen at position 4 completes the interactions made by the chromen-4-one by receiving two H-bonds from an amino group of Arg14 and a water molecule that is in turn H-bonded to the NADPH/NADP$^+$β-phosphate O2. These interactions, together with the stacking of the chromen-4-one described above, bring its 3 position hydroxyl group within H-bonding distance of the backbone carbonyl oxygen of Leu208.The phenyl ring in position 2 on the chromen-4-one establishes a T-shaped stacking interaction with the aromatic side chain of Trp221 and forms van der Waals interactions with the side chains of Val206 and Leu209 (not shown). The *meta*-hydroxyl group at the 3' position on the phenyl moiety of **2** is only involved in a water mediated H-bond network linking it to the backbone carbonyl of Gly205 and the side chain of Asp161 (not shown).

***Tb*PTR1-NADPH/NADP$^+$-7.** The structure of *Tb*PTR1 in complex with NADPH/NADP$^+$ and compound **7** has been determined at 1.76 Å resolution. Ligand placement and key interactions within the active site cavity are shown in Figure 2D, where it can be observed that compound **7** adopts exactly the same pose as compound **2**, making the same interactions with the enzyme and cofactor. The only difference consists in the steric repulsion of the additional hydroxyl group at position 4' that

causes the side chain of Trp221 to move away by about 1.4 Å to make room for this group. The 4' hydroxyl group is not involved in H-bonds but is solvent exposed and presumably can form aH-bond with water.

The superposition of the four crystal structures is shown in Figure 5. The orientation of compounds **2** and **7** in the *Tb*PTR1 cavity is the same as for **NP-13,** with the inhibitor bicyclic core directed towards the opposite side of the cavity with respect to **NP-29.** Due to the larger steric hindrance of the substituents on the 2-o-methoxy-phenolring of **NP-13**, a little rearrangement of the whole molecule occurs with a rotation of about 35° of the bicyclic core with respect to **2** and **7** that allows the side chain of Trp221 to remain in the position observed in the *Tb*PTR1-**2** complex (Figure 2C). The rotation of **NP-13** allows direct H-bonding between the 3' hydroxyl group of **NP-13** and Asp161, while the interaction of the corresponding group of **2** and **7** is mediated by a water molecule. The displacement of the Trp221 side chain occurring upon binding of compound **7** can be appreciated (Trp221 as yellow sticks in Figure 5).

A puzzling aspect of all four crystal structures is that the different inhibitors have been systematically observed bound to three of the four *Tb*PTR1 subunits, whereas the NADPH/$NADP^+$ cofactor is found bound to all subunits in three instances out of four, although with lower occupancy in those subunits where the inhibitor is absent. The absence of the inhibitor is correlated with larger disorder in the substrate binding loop that brings Trp221 into the active site cavity. However, this loop always shows temperature factors higher than average, even in the subunits where both cofactor and inhibitor are bound. The disorder of this region is independent of the crystal packing since, when the loop is disordered (e.g. in subunit C in *Tb*PTR1-**NP-29**), it approaches the symmetry-related subunits in the same way as the ordered loop (e.g. in subunit A in *Tb*PTR1-**NP-29**) located on the opposite face of the *Tb*PTR1 tetramer. Confirming this observation, the other two ordered loops (e.g. in subunits B and D in *Tb*PTR1-**NP-29**) do not make close intermolecular contacts. In summary, we conclude that stabilization due to the π-stacking between the 2-aromatic ring of the inhibitor and the side chain of Trp221 is critical for the ordering of the substrate binding loop.

Computational docking of synthetic compounds to TbPTR1 and LmPTR1 and SAR analysis

Docking studies were conducted to further expand the SAR to all the hydroxylation/methoxylation patterns in the synthesized compounds. In addition, computational docking allowed the evaluation of possible binding modes and a corresponding SAR for *Lm*PTR1, for which no crystal structure with these compounds could be solved.

Like the crystallographic studies, computational docking showed multiple possible binding modes for the chromen-4-one system, which roughly group into three classes: (1) a typical substrate-like binding mode involving H-bonding with the NADPH/$NADP^+$ cofactor and Ser95 of *Tb*PTR1 (or Ser111 of *Lm*PTR1), as observed in the complexes of compounds **2**, **7** and **NP-13**; (2) an alternative binding mode with chromen-4-one flipped by roughly 180° as observed in the complex with **NP-29**; and (3) an inverse binding mode solely observed in docking studies, with ring B rather than the chromen-4-one in a stacking orientation between the NADPH/$NADP^+$ nicotinamide and Phe97 of *Tb*PTR1 (or Phe113 of *Lm*PTR1). While three of the four crystal structures feature binding mode (I), a general dependence of the binding mode on the substituent pattern is notable both from crystallographic and docking studies. In docking, many of the observed binding modes were found to have highly similar contacts and H-bonding partners, thus creating a favorable entropic contribution to the binding of this compound class (see also Tables S5 and S6 in Supporting Information). However, due to their large number of H-bond donors/acceptors, flavonoids can adopt additional binding modes with different, often water mediated, interactions. We therefore used a ligand constraint docking approach to favor arrangements close to the crystal complexes to assess the potential of other synthetic derivatives to bind in similar orientations.

The crystal structures and docking indicate that hydroxylation patterns on ring A influence the orientation of chromen-4-one in the pocket. Precisely, compounds hydroxylated at position R6 show different H-bonding partners (mostly NADPH/$NADP^+$ phosphate and Ser95/Ser111 of *Tb*PTR1/*Lm*PTR1, respectively) from those hydroxylated at R7 (mostly NADPH/$NADP^+$ ribose and

Tyr174/Tyr194 or *Tb*PTR1/*Lm*PTR1, respectively), see Figure 5. This difference also affected the compound activity (compare R6-hydroxylated compound **2** (96% *Tb*PTR1 inhibition at 50 μM) and the corresponding R7-hydroxylated compound **3** (47% *Tb*PTR1 inhibition at 50 μM)). While the geometry of compound **2** fits ideally in the *Tb*PTR1 binding pocket, the slight reorientation observed for compound **3** leads to a loss of H-bonds and stabilizing hydrophobic contacts, halving the compound activity. Thus, hydroxylation of ring A can fine-tune the arrangement of the chromen-4-one system within the pocket and critically influence the interaction pattern of rings B and C.

Methoxylations, in contrast to hydroxylations, were found to lead to activity loss. For example, the inhibitory activity against *Tb*PTR1 and *Lm*PTR1 drops substantially, when comparing compound **2** with the corresponding methoxylated compound **10** (96% and 4% *Tb*PTR1 inhibition at 50 μM; 86% and no *Lm*PTR1 inhibition, respectively). Methoxylations on the A-ring cause a displacement of the chromen-4-one from the primary stacking geometry to accommodate the bulkier methoxy-group in close proximity tothe NADPH/$NADP^+$ cofactor and Ser95 of *Tb*PTR1 (Ser111 of*Lm*PTR1), see Figure 6A. Notably, this adverse effect was also apparent in the comparison of compounds **1** and **9**, bearing no substitution on ring A but a hydroxylation or methoxylation on R3' of the B-ring. Whereas the activity of compound **9** is negligible, compound **1** shows about 35% inhibition against both *Tb*PTR1 and *Lm*PTR1 (at 50 μM). AH-bond donor functionality on R3' has an important stabilizing effect, as it can interact with a water molecule bridging Asp161 and Gly205 of *Tb*PTR1 (see Figure 6B) orAsp181 and Gly225 of *Lm*PTR1. As, according to our WatCH analysis, this water is almost 100% conserved in both *Tb*PTR1 and *Lm*PTR1, it provides a clear advantage for R3' hydroxylated compounds. This is further supported by the crystal structures of *Tb*PTR1 with compounds **2** and **7**, where the R3' hydroxylation is in H-bonding distance to this water site. In agreement with this observation, compound **2** with the m-hydroxyphenyl was over 30 times more active than compound **5** with a p-hydroxyphenyl ring (96% and 3% *Tb*PTR1 inhibition at 50 μM, respectively). In contrast to a meta-hydroxylation, a p-hydroxylation cannot interact with the structural water, see Figure 5. Again, this effect was sensitive to the hydroxylation pattern of ring A, as can be seen by comparing

compounds **3** (R3' and R7 hydroxylation, 47% *Tb*PTR1 inhibition at 50 μM) and compound **6** (R4' and R7 hydroxylation, 33% *Tb*PTR1 inhibition at 50 μM), see Figure 5. While p-substituted compounds generally show a drop in inhibitory activity compared to their respective m-substituted counterparts, the effect is weaker for the second pair with the R7 hydroxylation on ring A, possibly because R7 substitutions lead to a slight rotation of the stacking chromen-4-one, directing the p-hydroxyl towards a more solvent-exposed region of the pocket. In conclusion, the effects of individual hydroxyl substituents are not purely local and do not show a completely additive effect; rather, the combinations of ring A and B hydroxylations will determine the final binding mode.

Based on the binding modes observed for *Tb*PTR1, we evaluated possible binding orientations to *Lm*PTR1 by docking. Notably, all compounds with R4' hydroxylation (compounds **5** and**6**), compounds with R3' and R4' hydroxylations (compounds **7**and **8**) and one compound with R3' hydroxylation combined with an R7 substitution on ring A (compound **3**) were found to be slightly more active towards *Lm*PTR1 than *Tb*PTR1. While the depth of the biopterin binding pocket is well conserved and the interactions for chromen-4-one are practically identical in both proteins, there are notable differences towards the opening of the pocket that can explain the observed activity differences (see sequence alignment of interaction partners in Figure S2 of the Supporting Information). While in *Tb*PTR1, R3' hydroxylations on the B-ring mainly come into contact with the conserved water molecule and Cys168 (see Figure 5) and R4' hydroxylated compounds can hardly form direct H-bonds with the receptor, *Lm*PTR1 generally has a more polar opening part of the pocket. Three major differences are crucially important: His241, Tyr283 and Arg287 from the neighboring subunit in *Lm*PTR1, correspond to Trp221, Leu263 and His267 from the neighboring subunit in *Tb*PTR1, thereby providing several additional polar contact points. As the side chain of Arg287 in *Lm*PTR1 is much bigger than that of His267 in *Tb*PTR1, arginine is much more accessible to the ligands than histidine. Furthermore, as observed in crystal structures of *Tb*PTR1, Trp221 is rather motile and different rotamers lead to an open or a rather closed form of the pocket, thereby potentially blocking ligand access to His267. While Trp221 of *Tb*PTR1 did not provide aH-bonding

contact to any of the studied compounds, induced fit docking studies of the compounds to *Lm*PTR1 showed movement of His241 to allow additional H-bonding interactions in the most stable structure, as also shown in Figure 7 (see also Table S5). Overall, π-π stacking and hydrophobic contacts are clearly the main stabilizing factors for flavonoids in *Tb*PTR1, whereas a tendency towards a higher number of H-bond donor/acceptor contacts may stabilize hydroxylations in both the meta- and para-positions of ring B slightly better in *Lm*PTR1.

While addition of a para-hydroxylation for the R7 substituted ring A did not lead to a significant change in activity against *Tb*PTR1 (compound **3**: 47% and compound **8**: 53%*Tb*PTR1 inhibition at 50 μM), compound **4** with hydroxylations at R3', R4' and R5' yielded a clear activity increase (85% *Tb*PTR1 inhibition at 50 μM). Considering the lack of direct polar contact points in *Tb*PTR1, this is surprising and there may be two possible explanations: (1) bridging water molecules may enable additional contacts for the second meta-hydroxylation, e. g. with Trp221, or (2) the compound may adopt an inverted binding mode, placing the pyrogallol moiety in a stacking orientation with Phe97 and the cofactor, where it could make strong H-bonds and thereby keep the more hydrophobic chromen-4-one in the hydrophobic *Tb*PTR1 sub pocket, where it is able to form additional hydrophobic contacts.

Testing of synthetic flavonols against *Tb*DHFR, *Lm*DHFR, hDHFR and hTS

The compounds showing inhibitory activity against PTR1 (**1-8**) were evaluated for their activity against *Tb*DHFR, *Lm*DHFR and hDHFR, the results are given in Table S7 of the Supporting Information. With the exception of compounds **1** and **2**, all the tested compounds had inhibitory activities against *Tb*DHFR and *Lm*DHFR below 25% at 50 μM. Compounds **1** and **2** slightly inhibit, respectively, *Tb*DHFR and *Lm*DHFR (42-43% at 50 μM). Therefore, we conclude that compounds **1-8** have low inhibitory activity against the parasitic DHFRs. With the exception of compound **2**, all the compounds had inhibitory activities against hDHFR below 30 % at 50 μM. The IC_{50} of compound **2**

against hDHFR is 50 μM and against *Tb*PTR1 is 4.3 μM, thus compound **2** has a selectivity index higher than 10. None of the tested compounds inhibited hTS at 50 μM (data not shown).

Early toxicity studies

To characterize the compounds properties and to define their toxicological profile, we used an assay panel typical of those employed in drug discovery projects for hit/lead selection.[32] Our panel includes hERG, five cytochrome P450s, (CYP1A2, CYP2C9, CYP2C19, CYP2D6 and CYP3A4), Aurora B kinase, A549 (human lung adenocarcinoma epithelial) and WI-38 (foetal lung fibroblasts) cell lines and mitochondrial toxicity. The results of the screening are reported in Figure 8 as a traffic light code (from red through yellow to green for increasing biological effect and decreasing toxicity of the compounds) and in Table S8 of the Supporting Information. An ideal lead compound should have all parameters colored in green. In details, the percentage of mitochondrial toxicity and of inhibition towards hERG, CYP isoforms and Aurora B kinase should be below 30 %, while the percentage of A549/WI-38 cells growth, measuring cytotoxicity, should be above 70%. A few compounds showed a percentage of inhibition towards hERG >10 % at 10 μM. Apart from compounds **4** and **8**, all the compounds inhibited at least one isoform of cytochrome P450 (mostly CYP1A2), while only two compounds (**4** and **8**) exhibited a significant inhibitory activity against Aurora B kinase at 10 μM. None of the compounds was either cytotoxic or show mitochondrial toxicity.

Testing of synthetic compounds on cultured parasites

With the exception of compound **8**, all the molecules were tested at 10 μM against *T. brucei* bloodstream form, intracellular *T. cruzi* and *L. infantum* intracellular amastigotes (Figure 9). Almost all tested compounds were active against *T. brucei*, while only two compounds, **4** and **12,** were slightly active against *L. infantum* showing inhibitory activities of 10 and 35%, respectively. Twelve compounds (**1**, **2**, **5-12**, **14-16**) presented EC_{50} values against *T. brucei* between 1-8 μM (Table 2), while compounds **3**, **4** and **13** showed EC_{50} values of 12.29, 18.04 and 20.12 μM, respectively. Only the methoxylated compounds **10**, **11**, **14** and **16** showed antiparasitic activity towards *T. cruzi*

trypomastigotes similar to that of nifurtimox (NFX), the reference drug for the treatment of Chagas' disease. Compound **10** is the most active (EC_{50} = 4.5 μM, NFX EC_{50} = 1.6 μM).

The series was assessed for cytoxicity on THP1 macrophage-like cells to evaluate the NOAEL (no observed adverse effect level). The reference compound was pentamidine with a NOAEL of 10 μM and a selectivity index of 6440. The selectivity indexes of our compounds, given by the ratio between the EC_{50} towards *T. brucei* and CC_{50} towards THP1, were lower than 10 with the exception of compound **12** (SI = 17) (Table 2). The selectivity index acceptable for a compound to be considered non toxic[33] is at least 10, thus our compounds showed slight toxicity.

Combination studies and evaluation of synergy

All compounds were evaluated in combination with MTX independently of their PTR1 inhibitory activity against the recombinant protein. We aimed to assess the potential gain in potency and the reduction in toxicity through the combination of our compounds with MTX, a well-known DHFR inhibitor. In trypanosomatids MTX is expected to exert a synergistic behavior in combination with PTR1 inhibitors. Moreover, MTX can show a synergistic effect in combination with non-PTR1 inhibitors through a multitarget inhibition. Preliminary combination experiments in *T. brucei* were conducted by fixing MTX at 4 μM (MTX average EC_{30} against *T. brucei*) and varying the concentration of the selected compounds between 1.25 and 20 μM (Table S10 of Supporting Information). The synergy coefficients of all the compounds tested at the different concentrations (1.25, 2.5, 5, 10, 20 μM) are reported in Table S11 of the Supporting Information. Eight compounds presented a synergistic effect (synergy coefficient > 1) when combined with MTX. The anti-parasitic activity against *T. brucei* of the eight compounds both alone and in combination with MTX is shown in Figure 11. Compounds **5**, **6** and **13** consistently presented the highest synergy coefficients (maximum synergy coefficient > 1.5). Compound **13** was the most synergic with a calculated maximum synergy coefficient of 3.1 at 1.25 μM (Table S11). Since it showed the highest synergy

coefficient together with a safe toxicological profile (Figure 8, the only poor (red) parameter is for CYP1A2 (72% inhibition at 10 μM)), it was selected for further synergistic combination studies.

To better evaluate the gain in potency of the combination MTX-**13**, we employed the software Compusyn and a constant ratio between the concentrations of the two compounds chosen from their EC_{50} values (EC_{50} **13** = 20 μM; EC_{50} MTX = 15; constant ratio = 1.3)[34] This enabled us to quantify synergism between the two compounds (combination index- CI) and to determine the dose reduction (dose reduction index - DRI) needed to observe the studied effect in the combination compared with the dose of each drug alone. The combination of MTX and compound **13** at the EC_{50} concentration had a CI of 0.174 ± 0.047. When CI is lower than 1, the combination can be considered synergistic, therefore the observed CI is showing strong synergism and confirms the initial data (Table S10). At higher EC values, CI becomes lower indicating very strong synergism (Table 3). The EC_{50} determined for the combination showing CI of 0.147 was 3.15±0.33 μM. This enabled an average DRI at the EC_{50} of 14.6±3.7 for MTX and of 11.7±2.7 for compound **13** (IC_{50} MTX = 1.3 μM and IC_{50} **13** = 1.7 μM) (Figure S3C Supporting Information). At the EC_{90} of the mixture the predicted DRI is over 100-fold for both compounds when compared with the EC50 of the compounds alone. The isobologram is reported in Figure S3 of the Supporting Information. The toxicity of the MTX-**13** mixture on THP1 was determined at three different concentrations (12.5, 25, 50 μM) and no synergistic toxicity on human cells was observed (Figure S4 and Table S12). Therefore, the identified combination MTX-**13** is selective for the inhibition of the parasite growth, while there is no synergy in the toxicity towards the host cells. These data together with the predicted DRI indicate that the combination improves the selectivity indexes for both MTX and compound **13**.

Pharmacokinetic studies, *in-vivo* assays and compound delivery

Compound **2** was selected for pharmacokinetic studies because it was the most active compound against *Tb*PTR1 (IC_{50}= 4.3 μM) that showed activity against the parasite *T. brucei* (EC_{50}= 7.6 μM) and it presented a safe profile, see Figure 8. The hERG IC_{50} (99.3 μM) was more than 20-fold higher

than the target IC_{50}. With the exception of the CYP1A2 IC_{50} (6.1 μM), the IC_{50} against the cytochrome isoforms was higher than 10 μM. The solubility of compound **2** was evaluated using UV-Vis spectroscopy. *In-vivo* bioavailability and half-life of compound **2** were evaluated in BALB/c mice treated IV with 1 mg/kg based on its low solubility. The molecule showed a short half-life ($t_{1/2}$ = 7.6 min) and it was not detected in blood after 30 minutes (the plasma levels are shown in Figure S4 of the Supporting Information). With the aim of improving the plasma levels of compound **2**, we used two different drug delivery systems: the molecule was encapsulated in PLGA nanoparticles and solubilized with hydroxypropyl-β-cyclodextrins. The encapsulation did not change the physical properties of the PLGA nanoparticles as reported in Table S13 of the Supporting Information. The unloaded and loaded NPs were characterized by Dynamic Light Scattering (DLS) in terms of size, polydispersity index and zeta-potential. We evaluated the *in-vivo* bioavailability of compound **2** encapsulated in nanoparticles in BALB/c mice (IV and per os administration) and formulated with cyclodextrins after per os administration to NMRI mice. From preliminary data, both formulations did not significantly increase the levels of compound **2** in plasma samples from mice (data not shown). However, the *in-vitro* activity of compound **2** both in PLGA and in the cyclodextrin solution was preserved when compared to the free compound, while the toxicity on THP1 was diminished (Table 4).

Conclusion

This is the first study in which we have confirmed the potential of flavonols as PTR1 inhibitors. Apart from compounds **4** and **8**, none of the sixteen synthesized flavonols have previously been reported in literature for their antiparasitic activity.[22] Twelve of these compounds show EC_{50} values against *T. brucei* below 10 μM. We performed combination studies with MTX and compound **13**, a non-PTR1 inhibitor, was the best-performing compound. Although the reason for the synergy is unknown, compound **13** is an interesting compound for drug development due to the synergistic behavior with MTX and the low toxicity on host cells. Target identification studies could be carried out aiming to

explain the mechanism of action. The synthesized compounds were also evaluated for the activity against *T. cruzi* trypomastigotes and compound **10** turned out to have a potency comparable to that of nifurtimox, the drug currently used to treat Chagas' disease (EC_{50} compound **10** = 4.5 μM, NFX EC_{50} = 1.6 μM). We carried out early *in-vitro* toxicity assays and overall the library showed a satisfactory profile. Combining the activity/toxicity data, we selected compound **2** for pharmacokinetic studies and we observed a very quick turnover of the molecule in BALB/c mice. Neither encapsulation in PLGA nanoparticles nor solubilization with cyclodextrins increased the plasma level of compound **2**; however, both formulations allowed to maintain the *in-vitro* activity of the compound and to reduce the toxicity. Our crystal structures and SAR analysis provide a basis for structure-based drug design aimed at identifying novel flavonol-like compounds with increased potency and selectivity towards PTR1 and able to overcome the problems of classical flavonols.

Experimental section

Preparation of the natural products library

A library of 98 natural compounds, consisting of 8 flavanones, 19 flavones, 20 flavonols, 2 dihydroflavonols, 13 anthocyanins, 2 catechins, 2 isoflavones, 4 chalcones, 18 phenolic acids and derivatives, 1 aurone, 5 anthraquinones, 3 triterpenes and 1 phloroglucinol was purchased from Extrasynthese (Genay, France) and Sigma-Aldrich-Fluka (Milan, Italy) for drug screening. The degree of purity of all these molecules was checked by HPLC. The HPLC analyses were performed on an Agilent Technologies (Waldbronn, Germany) modular model 1100 system, consisting of a vacuum degasser, a quaternary pump, an autosampler, a thermostated column compartment and a diode array detector (UV/DAD). The chromatograms were recorded using an Agilent Chemstation for LC and LC-MS systems (Rev. B.01.03).An Ascentis C_{18} column (250 × 4.6 mm I.D., 5 μm, Supelco, Bellefonte, PA, USA) was used, with a mobile phase composed of (A) water (H_2O) and (B) acetonitrile (ACN). The gradient elution was modified as follows: 0-3 min 25% B, 3-10 min from 25 to 30% B, from 10-40 min from 30 to 40% B, which was held for 5 min. The post-running time was 5

min. The flow-rate was 1.0 mL/min. The column temperature was set at 30 °C. The sample injection volume was 5 µL. The UV/DAD acquisitions were carried out in the range 190-600 nm and chromatograms were acquired at 310, 330, 370 and 520 nm. All the compounds tested were found to be stable and degradation products were not detected in the HPLC chromatograms. Table 1 of the Supporting Information shows the purity (> 95%) of the 38 natural compounds screened. The natural compounds were stored at low temperature (-80 °C), protected from light and humidity.

Computational studies

Virtual screening of the natural product library

The library of 98 natural products was subjected to virtual screening using the GOLD software (version 5.1)[35,36] following the protocol validated in previous studies on PTR1.[13] The compounds were docked into the binding sites of the targets, *Lm*PTR1 (PDB id: 1E92) and *Tb*PTR1 (PDB id: 3JQ9), and the off-targets, hDHFR (PDB id: 1U72) and hTS (PDB id: 1HVY). Ten docking poses were generated for each ligand in each target and these were visually inspected and manually ranked, considering the Gold fitness score, hydrogen bonding and π-π aromatic interactions. A search of BioAssay data in PubChem was done to filter out promiscuous compounds. The set of 38 compounds given in Table 1 of the Supporting Information was selected for inhibition assays considering the above properties and structural diversity.

Docking of synthetic flavonoid derivatives

The 3D structures of the compounds were created from SMILES strings and optimized with the OPLS_2005force field usingMaestro.[37] Ionization states and tautomers were generated at pH 7.0±0.5 using Epik.[37] Up to 8 stereoisomers and one low-energy ring conformation were generated per compound. Important structural water sites were identified using the WatCH clustering approach.[38] All available chains of the *Lm*PTR1 crystal structures and 99 chains from *Tb*PTR1 crystal structures (see Tables S14 and S15 for a list of structures) were superimposed and their water sites were

clustered with a distance criterion of 2.4 Å for considering a water oxygen position identical. Water sites with at least 50% conservation were considered conserved.

The PTR1 structures for docking consisted of chain A of the relevant crystal structure and a C-terminal tripeptide from the neighboring subunit pointing into the chain A active site (Val266 to Ala268 in*Tb*PTR1 and Thr286 to Ala288 in *Lm*PTR1). The side-chain oxygen atom on the modified Cys 168 in the crystal structure of *Tb*PTR1 was removed. Crystallographic solvent molecules were removed and replaced by the conserved water molecules identified by WatCH clustering. The *Lm*PTR1 structure (PDB ID 1E92) was aligned to the *Tb*PTR1 template (PDB id 5JCJ). PrepWizard was used to assign bond orders and add hydrogen atoms.[37] The N- and C-termini of chain A were capped with N-acetyl and N-methyl amide groups, respectively. The protonation state of the NADPH/$NADP^+$ cofactor was computed at pH 7.0±0.5. Protein protonation states were assigned by PROPKA[43] at pH 7.0. The H-bond network was optimized and all hydrogens were subjected to a restrained minimization. A 20 Å x 20 Å x 20 Å docking grid was centered on Phe97 of*Tb*PTR1 orPhe113 of*Lm*PTR1. The following hydroxyl groups were set rotatable: Ser95 and Tyr174 in *Tb*PTR1 and Ser111, Thr184, Tyr191, Tyr194, Thr195 and Tyr283 in*Lm*PTR1, as well as those of the NADPH/$NADP^+$ ribose.

Docking was performed with and without ligand-based constraints using the Glide software.[39-42] For the ligand constraints, protein preparation was performed including compound **7** (substrate-like binding mode, PDB ID 5JCJ) or compound **NP29** (inhibitor-like binding mode, PDB id 5JCX) or the highest scoring docking solution from unconstrained docking of compound **4** with ring B in a stacking orientation (alternate binding mode). The ligands were then separated from the structure to provide reference geometries. The van der Waals radii of the ligand atoms were scaled by 0.80 and a partial charge cut-off of 0.15 was used. XP (extra precision) docking and flexible ligand sampling were set. Nitrogen inversions and ring conformations were sampled, biased sampling of torsions was performed for amides only and set to penalize a non-planar conformation. Epik state penalties were added to the

docking score, intramolecular H-bonds were rewarded and the planarity of conjugated π groups was enhanced. A core pattern comparison with a tolerance of 3Å was used for the ligand-based constraint. The core was defined as all non-hydrogen atoms of the chromen-4-onecore ring system except the R3 hydroxyl group. 20 poses per ligand were subjected to post-docking minimization with a threshold of 0.5 kcal/mol for rejecting a minimized pose. Up to 10 final docking solutions were reported. Unconstrained docking was performed analogously, omitting only the core pattern comparison. For *Lm*PTR1, the core constraint docking was based on the binding poses in *Tb*PTR1. In addition, induced-fit docking was carried out using the same settings except that the size of the docking grid was chosen automatically and a ligand and receptor van der Waals scaling of 0.5 was applied. Refinement was carried out with Prime[37] for residues within 5 Å of the ligand, followed by XP re-docking into structures within 30 kcal/mol of the best structure and within the top 20 structures overall. Up to 20 final docking solutions were reported.

Synthesis

General. All commercial chemicals and solvents were reagent grade and were used without further purification. Reaction progress was monitored by TLC on pre-coated silica gel 60 F254 plates (Merck) and visualization was accomplished with UV light (254 nm). ^{1}H and ^{13}C NMR spectra were recorded on a Bruker FT-NMR AVANCE 400. Chemical shifts are reported as δ values (ppm) referenced to residual solvent ($CHCl_3$ at δ 7.26 ppm, DMSO at δ 2.50 ppm, MeOD at δ 3.31 ppm); *J* values were given in Hz. When peak multiplicities are given, the following abbreviations are used: s, singlet; d, doublet; t, triplet; q, quartet; m, multiplet; br, broadened signal. Silica gel Merck (60-230 mesh) was used for column chromatography. Purity of the compounds was assayed by means of TLC (Merck F-254 silica gel). Mass spectra were obtained on a 6520 Accurate-Mass Q-TOF LC/MS and 6310AIon TrapLC-MS(n). The detailed NMR and mass data of the synthesized compounds are reported in the Supporting Information (Pag. 33-37).

General procedure for the synthesis of (2E)-1-(2-hydroxy-phenyl)-3-phenylprop-2-en-1-ones.

An aqueous solution of NaOH (3 M, 1.6 mL) was added to a solution of aromatic ketone (1 mmol) and substituted benzaldehyde (1.2 equiv.), in EtOH (1-2 mL). The reaction was stirred at room temperature overnight. The reaction mixture was cooled in an ice-water bath and acidified to pH 2 with concentrated HCl (37%). The solid formed was filtered, washed with ethanol and then further purified by recrystallization from EtOH.

General procedure for the synthesis of methylated flavonols (compounds 9-16).

An aqueous solution of H_2O_2 (30%, 250 μL) was added to an ice-cold suspension of the chalcone (1 mmol) in ethanol (5 mL) and 1 M NaOH (2 mL). The mixture was allowed to warm to room temperature and was stirred for 5-18 hours. Then the reaction mixture was cooled in an ice bath and distilled water (2-4 mL) was added. Concentrated HCl (37 %) was added until pH 2 and the precipitate was filtered, washed with EtOH and further purified by recrystallization from EtOH. When no precipitate occurred, the reaction mixture was extracted with dichloromethane and washed with water and brine. The organic layer was dried over Na_2SO_4 and concentrated under reduced pressure. Column chromatography was utilized to purify the desired product.

General procedure for the synthesis of demethylated flavonols (compounds 1-8).

To a stirring solution of **15** (0.500 g, 1.52 mmol) in anhydrous dichloromethane (30 mL) under nitrogen at 0°C, boron tribromide in dichloromethane (1.0 M, 13.7 mL, 13.7 mmol, 9 eq) was added. The mixture was allowed to warm at room temperature and was stirred for 2 days. The reaction mixture was then cooled to 0°C and methanol (10 mL) was added. The reaction mixture was concentrated *in vacuo*. Water (10 mL) was added, the reaction sonicated and then left to stand. Compound **7** (0.440 g, quantitative yield) was collected as a red solid.

The procedure followed for the synthesis of all demethylated flavonols is analogue to that of compound **7** considering 3 eq of BBr_3 for each C-O bond cleavage.

Protein expression and purification

Recombinant *Tb*PTR1 was expressed and purified by established methods[10] with minor revisions. The plasmid was supplied by Prof William N. Hunter University of Dundee. Briefly, protein expression

was carried out in *E. coli*BL21(DE3) cultured at 37°C in SuperBroth (SB) medium to mid-log phase and induced with 1 mM isopropyl-β-d-thiogalactopyranoside (IPTG) overnight at 30°C.[27] Cells were resuspended in 50 mM Tris-HCl, pH 7.5, 250 mM NaCl and disrupted by sonication. The target protein purification was achieved in a single step using a HisTrap FF 5mL column (GE-Healthcare) and an imidazole concentration of 250 mM in the same buffer. The resulting protein sample was dialyzed overnight in 20 mM Tris-HCl pH 7.5 at 8°C (membrane cutoff 10 kDa). The high purity of the sample was confirmed by SDS-PAGE analysis and MALDI-TOF mass spectrometry. The final protein yield of enzyme was established as approximately 50 mg L^{-1}bacterial culture.

The plasmid pET15b-*Lm*PTR1 was supplied by Prof William N. Hunter University of Dundee. Protein expression was performed in the *E. coli* strain BL21(DE3)cultured at 37°C in SB medium (supplemented with 100 mg/L ampicillin)to mid-log phase and induced with 0.4 mM IPTG for 16 h at 28 °C. Cells, harvested by centrifugation were resuspended in buffer A (50 mM Tris-HCl pH 7.6, 20 mM imidazole and 250 mM NaCl) and disrupted by sonication. The supernatant, collected by centrifugation, was further purified by nickel-affinity chromatography (HisTrap FF 5mL column, GE-Healthcare) and the target protein was eluted using a 250-500 mM imidazole concentration in the same buffer. Fractions containing the protein (identified by SDS-PAGE) were pooled and combined with thrombin protease and then dialyzed overnight in 50 mM Tris-HCl pH 7.6 at 25°C. The mature protein was purified by a second nickel-affinity chromatography (HisTrap FF 5mL column, GE-Healthcare) and eluted as weakly bound protein, in 50-100 mM imidazole and 50 mM Tris-HCl pH 7.6. The resulting protein sample was dialyzed in 20 mM sodium acetate pH 5.3 and 10 mM DTT. The high purity of the sample was confirmed by SDS-PAGE analysis and MALDI-TOF mass spectrometry, and the final protein yield established as approximately 30 mg/L bacterial culture.

Recombinant *Lm*DHFR-TS was cloned in our lab. The gene coding sequence for *Lm*DHFR-TS, cloned in pET-15b expression vector, was introduced by thermal shock into the *E. coli* strain ArcticExpress(DE3). Bacterial culture was grown at 30°C in ZYP-5052 autoinduction medium

(supplemented with ampicillin 100 mg/L) to OD_{600nm}value of about 1 and then cell growth was continued for 60 at 12°C under vigorous aeration. Cells, harvested by centrifuge , were resuspended in buffer A (50 mM sodium Citrate pH 5.5 and 0.25 M NaCl) and disrupted by sonication. The supernatant of the resulting crude extract was collected by centrifuge and purified by nickel-affinity chromatography. The target protein was eluted using a linear gradient 20-250 mM imidazole in the same buffer. Fractions containing the target protein (identified by SDS-PAGE) were pooled and dialyzed overnight in buffer A at 8°C. The resulting protein sample was further purified on a gel filtration column (HiLoad 16/600 Superdex 200pg, GE Healthcare) equilibrated with 50 mM sodium citrate pH 5.5 and 0.25 M NaCl). The high purity of the target protein was confirmed by SDS-PAGE analysis and the final yield established as approximately 10 mg/L bacterial culture.

The recombinant *Tb*DHFR-TS was cloned in our lab. The synthetic gene encoding for *Tb*DHFR-TS, optimized for *E. coli* expression and cloned in pET-15b expression vector was purchased from GenScript USA Inc. The target protein was expressed and purified using the same protocol described for *Lm*DHFR-TS, with minor modification. Briefly, cells were resuspended in buffer A (50 mM phosphate buffer pH 7.5, 0.25 M NaCl, 10% glycerol, and 20 mM imidazole) and disrupted by sonication. The supernatant of the resulting crude extract was collected by centrifuge and purified by nickel-affinity chromatography (HisTrap FF 5mL column, GE-Healthcare). The target protein was eluted using a 400 mM imidazole concentration in the same buffer. Eluted fractions were pooled and dialyzed overnight in buffer A at 8°C. The resulting protein sample was concentrated and applied to a gel filtration column (HiLoad 16/600 Superdex 200pg, GE Healthcare) equilibrated in buffer A. The high purity of the sample was confirmed by SDS-PAGE and the final protein yield established as approximately 8 mg/L bacterial culture. hTS and hDHFR were purified as reported in literature. [15,44]

The kinetic characterization (K_m and K_{cat}) of all the proteins purified and employed for the target/off target screening is reported in Table S16 of the Supporting Information.

X-ray crystallography

Crystals of histidine-tagged *Tb*PTR1 were obtained by the vapor diffusion hanging drop method technique at room temperature.[45] Drops were prepared by mixing equal volumes of protein (6-10 mg mL^{-1}in 20 mM Tris-HCl pH 7.5 and 5-10 mM DTT) and precipitant (1.5-2.5 M sodium acetate and 0.1 M sodium citrate pH 5) solutions and equilibrated over a 600 µL reservoir. Well-ordered monoclinic crystals grew in 3-6 days. The *Tb*PTR1-cofactor-inhibitor complexes were obtained by soaking crystals with each compound solubilized either in 1,4-dioxane or DMSO (without exceeding a dioxane-DMSO/crystal solution ratio of 1:9). After 4-21 hours crystals were transferred to a cryo-protectant, prepared by adding 30 % v/v glycerol to the precipitant solution, and flash frozen in liquid nitrogen. Diffraction data for the complexes with compound **NP-29** and **NP-13** were measured using synchrotron radiation at the Diamond Light Source (DLS, Didcot, United Kingdom) beamline I04 equipped with a Pilatus 6M-F detector, using a wavelength of 0.9795 Å, a 0.25° rotation and a 0.4 s exposure time/image. Data for the complex *Tb*PTR1-NADPH/$NADP^+$-**2** were collected at the DLS beamline I03 equipped with a Pilatus3 6M detector and using a wavelength of 0.9173 Å, a 0.25° rotation and a 0.15 s exposure time/image. Data relative to the complex with compound **7** were collected at the European Synchrotron Radiation Facility (ESRF, Grenoble, France) beamline ID30A-1, equipped with a Dectris Pilatus3 2M detector, and by using a wavelength of 0.9660 Å, a 0.1° rotation and a 0.08 s exposure time/image. X-ray images were integrated using Mosflm and scaled with SCALA within the CCP4 software suite.[46-48] *Tb*PTR1 crystals belong to the monoclinic space group $P2_1$, showing only slight variations in cell parameters among the different crystals. Data collection and processing statistics are reported in Table S2 (Supplementary Information). The structures were solved by molecular replacement using the software Molrep[49] and a whole tetramer of *Tb*PTR1 (PDB code 2X9G) as searching model.[50] Structural models were refined using REFMAC5[51], whereas the program Coot[52] was used for electron density inspection, model manipulation, and placement of the solvent molecules. The final models were inspected manually and checked with the programs Coot and Procheck.[53] Data refinement statistics are reported in Table S3. Figures were generated with CCP4mg.[54]

_Tb_PTR1, _Lm_PTR1, _Tb_DHFR, _Lm_DHFR, hTS and hDHFR target enzyme assays

The *in-vitro* assay used for PTR1 enzymes is based on the coupled assay reported by Shanks et al.[55] PTR1 uses H2B as a substrate and require also NADPH for the reaction, the reduction of H2B to H4B by PTR1 is non-enzymatically linked with the reduction of cytochrome c in this assay, which is detected at 550 nm. The formation of cyt c Fe^{2+} results in a signal increase in the photometric readout.

*Tb*PTR1 and *Lm*PTR1 activity was assayed in a buffer containing 20 mM sodium citrate (pH 6.0). The final reaction mixture contained test compound at a range of concentrations and *Tb*PTR1/*Lm*PTR1 (6.0 nM/12 nM), H2B (0.3 μM/3 μM), cytochrome c (100 μM/100 μM), and NADPH (500 μM/500 μM). The final assay volume was 50 μL in 384 well clear plates (Greiner bio-one, 781101). Compound screening was performed by addition of compound to assay plates (in 100 % DMSO) followed by addition of 45 μl Reaction Mix (enzyme, H2B cytochrome c in 20mM sodium citrate buffer). A pre-read was made at 550 nm using an EnVision® Multilabel Reader 2103 (PerkinElmer Inc, US) followed by incubation of the assay plates at 30 °C for 10 min. The reaction was initiated by the addition of 5 μl NADPH (5 mM in ultrapure water) followed by kinetically reading the assay plates at 550 nm using the EnVision® MultilabelReader at 10, 20, 30, 40 and 50 min and the slope of each assay well was calculated. The screening data was analyzed using ActivityBase (IDBS) and for outlier elimination in the control wells the 3-sigma method was applied. Based on the slope data was normalized to the positive control methotrexate for *Tb*PTR1/*Lm*PTR1 (1 μM/50 μM, yielding 100 % inhibition) and negative controls (1 % DMSO, yielding 0 % inhibition) and % inhibition calculated for all samples. The measurement at time 0 min was used to flag optically interfering samples. Each compound was tested in triplicate and the pIC50 value, Standard Deviation, Hill Slope, Minimum Signal and Maximum Signal for each dose-response curve were obtained using a 4-parameter logistic fit in the XE module of ActivityBase (IDBS).

*Lm*DHFR, hDHFR and hTS activities were assessed spectrophotometrically.[13] The Km for the substrates and *k*cat for all enzymes purified and used for the inhibition studies are reported in Table S16 of the Supplementary Information.

***In-vitro* biological assays**

A cloned line of *L. infantum* (MOM/MA671TMAP263) promastigotes were maintained in RPMI 1640 medium supplemented with 10 % heat-inactivated fetal bovine serum (FBS), 2 mM L-glutamine, 20 mM HEPES and 1 % Penn/Strep. Maintenance of promastigotes was done in T-25 flasks at 26 ºC by sub-passage at 10^6 parasites/mL every 5-6 days. *L. infantum* axenic amastigotes expressing episomal luciferase were maintained in MAA/20 (axenic amastigote medium) at 37 °C under a 5 % CO_2 environment with sub-passages every 5 days. *LUC*-positive parasites were selected by addition of geneticin sulphate (G418) to the culture at 60 μg/mL. *Trypanosoma brucei brucei* Lister 427 bloodstream forms were grown at 37 ºC, 5 % CO_2, in complete HMI-9 medium supplemented with 10 % fetal calf serum (FCS) and 100 UI/mL of penicillin/streptomycin. Cultures were diluted before a cell density of 2 x 10^6/mL was reached.

***In-vitro* evaluation of activity against *L. infantum* intramacrophage amastigotes**

The efficacy of compounds against *L. infantum* intracellular amastigotes was determined according to literature[56] but with slight modifications. Briefly, 1 x 10^6 THP-1-derived macrophages were infected with luciferase-expressing *L. infantum* axenic amastigotes in a macrophage:amastigotes ratio of 1:10 for 4 hours at 37 °C, 5 % CO_2. Non-internalized parasites were washed and compounds were added at different concentrations (20-0.6 μM). After 72 hours of incubation at 37 °C and 5 % CO_2, media was substituted by PBS. Macrophages were lysed by addition of 25 μL Glo-lysis buffer (Promega). Steady-Glo reagent (Promega) was then added and the content of each well was transferred to white-bottom 96-well plates. Luminescence intensity was read using a Synergy 2 Multi-Mode Reader (Biotek). The anti-leishmanial effect was evaluated by the determination of IC_{50} value (concentration required to inhibit growth in 50 %) and calculated by non-linear regression analysis using GraphPad

Prismversion 5.00 for Windows, GraphPad Software, San Diego California USA, www.graphpad.com.

In-vitro* evaluation of activity against *T. brucei

The efficacy of compounds against *T. brucei* bloodstream forms was evaluated using a modified resazurin-based assay previously described.[57] Mid-log bloodstream forms were added to an equal volume of serial dilutions of compounds in supplemented complete HMI-9 medium at a final cell density of $5x10^3$/mL. Following incubation for 72 hours at 37 °C 5 % CO_2, 20 µL of a 0.5 mM resazurin solution was added and plates were incubated for a further 4 hours under the same conditions. Fluorescence was measured at 540 nm and 620 nm excitation and emission wavelength, respectively, using a Synergy 2 Multi-Mode Reader (Biotek). The anti-trypanosomatid effect was evaluated by the determination of IC_{50} value (concentration required to inhibit growth in 50 %) and calculated by non-linear regression analysis using GraphPad Prism version 5.00 for Windows, GraphPad Software, San Diego California USA, www.graphpad.com. Half maximal inhibitory concentrations (IC_{50}) reported correspond to the averages of the results obtained in at least two independent experiments. Compusyn software 1.0 was used to evaluate synergy.[34]

In-vitro evaluation of activity against T. cruzi

Infections were performed in 6-well plates (3 x 10^6 HG39 cells/well). Confluent HG39 cells were infected with sanguineous trypomastigotes of *T. cruzi* Y strain at a 1:1 ratio. After 4 hours, the cells were washed three times with PBS and fresh medium was added (RPMI supplemented with Glut/Pen/Strep and 20 % heat-inactivated FCS, Sigma-Aldrich). The infected cells were incubated at 37 °C and 5 % CO_2). 24 hours post infection, the cells were treated with compounds and incubation was continued for 48 hours. The gDNAs of infected cells was isolated using the LGC genomics mag maxi kit following the manufacturer's (LGC Genomics, Berlin) protocol and used as a template for a TaqMan™ probe-based quantitative real-time PCR (Bifeld, E. et al., manuscript submitted). The reference gene and the gene of interest were amplified using the KAPA Probe Fast qPCR Master Mix

Kit (VWR) following the manufacturer protocol. Template DNA was used as 10 % of the final reaction volume. Primers specific for human ß-actin (reference gene) were human-beta-AcF2 (CCCATCTACGAGGGGTATG) and human-beta-AcR3 (TCGGTGAGGATCTTCATG). The parasite actin-specific primers were *T. cruzi*-AcF (CGTGAGAAGATGACACAG) and *T. cruzi*-AcR (GGGAGAGAGTATCCCTCG). All primers were used at a final concentration of 300 nM. The probe-specific for human ß-actin was human-beta-Ac probe (**Cy5**-CCTGGCTGGCCGGGACCTGAC-**BHQ-3)** labeled with the dye Cy5 at the 5'end and with the quencher BHQ-3 at the 3'end. The probe specific for parasite actin was *T. cruzi* Ac probe (**FAM**-CACGCCATCACCAGCATCAAG-**BHQ-1**) labeled with the dye FAM at the 5'end and with the quencher BHQ-1 at the 3'end. Probes were used in a final concentration of 200 nM. The program was adapted to the use with the KAPA™ Probe Fast qPCR Kit Master Mix.

Cytotoxicity assessment against THP-1 macrophages

The effect of compounds **1-16** on THP-1-derived macrophages was assessed by the colorimetric MTT assay (3-(4,5-dimethylthiazol-2-yl)-2,5-diphenyl tetrazolium bromide). Briefly, 1 x 10^6 THP-1 cells were differentiated into macrophages by addition of 20 ng/mL of phorbol-myristate 13-acetate (PMA, Sigma Aldrich) for 18 hours, followed by replacement with fresh medium for 24 hours. Cells were incubated with compounds ranging from 100 to 3 µM after dilution in RPMI complete medium containing a maximum amount of 1 % DMSO. After incubation for 72 h at 37 °C, 5 % CO_2, medium was removed and a 0.5 mg/mL MTT solution was added. Plates were incubated for additional 4 hours to allow viable cells to convert MTT into a purple formazan product. Solubilization of formazan crystals was achieved by addition of 2-propanol and absorbance was read at 570 nm using a Synergy 2 Multi-Mode Reader (Biotek). Cytotoxicity was evaluated by the determination of CC_{50} value (drug concentration that reduced the percentage of viable cells in 50 %) and calculated by non-linear regression analysis using GraphPad Prism version 5.00 for Windows, GraphPad Software, San Diego California USA, www.graphpad.com.

hERG cardiotoxicity assay

The Invitrogen Predictor™ hERG Fluorescence Polarisation Assay was used in 384 well assay format (Greiner bio-one, 784076) to test compounds. To each well of the assay plate, 100 nL of the test /control compound was added followed by addition of 5 µl of homogenized membrane solution (undiluted) was added followed by a further addition of 5 µl of tracer (1 nM final concentration in assay). The plates were incubated at 2 hours at 25 °C in an humidity controlled incubator and the Fluorescence Polarisation measured using an EnVision®Multilabel Reader 2103 (PerkinElmer Inc, US).The screening data was analyzed using ActivityBase (IDBS)and for outlier elimination in the control wells the 3-sigma method was applied. The negative controls (0 % inhibition) and positive controls E-4031, a blocker of hERG-type potassium channels (yielding 100 % inhibition) were used to normalize the raw data. Each compound was tested in triplicate and the pIC_{50} value, Standard Deviation, Hill Slope, Minimum Signal and Maximum Signal for each dose-response curve were obtained using a 4-parameter logistic fit in the XE module of ActivityBase (IDBS). All IC_{50} data were associated with <10 % SD.

Cytochrome P450 1A2, 2C9, 2C19, 2D6 and 3A4 assay

The luminescence based P450-Glo™ (Promega) was used in 384 well assay format (Greiner bio-one, 784076) to test compounds. The selected cytochrome P450 panel included microsomal preparations of cytochromes P450 1A2, 2C9, 2C19, 2D6 and 3A4 (Corning) from baculovirus infected insect cells (BTI-TN-5B1-4) which express cytochromes P450 (CYP) and cytochrome c reductase (and cytochrome b5 for 3A4).Compounds/controls were added into the empty 384 well plate (100 nL/ v/v 1% DMSO) using Echo® Liquid Handler (LabcyteInc) followed by addition of 5 µL/well of CYP/Luciferin- substrate and incubated for 30 min at 37°C. The reaction was initiated by addition of 5 µL/well NADPH regeneration mixture. After 30 min at 37°C the CYP reaction was stopped and the luciferase reaction was initiated by addition of 10 µl/well of Luciferin Detection Reagent. After additional 30 min at 37 °C, the luminescence readout was performed using the Infinite® M1000 PRO plate reader (Tecan).Outliers in the control wells were eliminated according to the 3-sigma method.

Negative controls (0 % inhibition)included only vehicle (v/v 1 % DMSO), standard specific CYP inhibitors [CYP 1A2 inhibitor α-naphtho-flavone (Sigma-Aldrich,15 nM), CYP 2C9 inhibitor sulfaphenazole (Sigma-Aldrich, 67 nM), CYP 2C19 inhibitor troglitazone (Sigma-Aldrich, 3.2 µM), CYP 2D6 inhibitor quinidine (Sigma Aldrich, 2 nM) and CYP 3A4 inhibitor ketoconazole (Sigma Aldrich,54 nM) were used aspositive controls (100 % inhibition). Each compound was tested in triplicate and the pIC50 value, Standard Deviation, Hill Slope, Minimum Signal and Maximum Signal for each dose-response curve were obtained using a 4-parameter logistic fit in the XE module of ActivityBase (IDBS). All IC_{50} data were associated with < 10 % SD.

Cytotoxicity assay against A549 and WI38 cells

These assays were performed using the CellTiter-Glo assay from Promega Corp.A549 cells obtained from DSMZ (German Collection of Microorganisms and Cell Cultures, Braunschweig, Germany) and WI-38 cells were obtained from ATCC (ATCC® CCL-75™) and were grown on surface modified T175 cell culture flasks (cat. no. 660175, Greiner Bio One GmbH, AT) in DMEM (cat. no. 41966-052, Life Technologies, US) with 10 % FCS, streptomycin (100 µg/mL) and 100 U/mLpenicillin G (cat. no. P-11-010, PAA Laboratories GmbH, AT). Cells were incubated at 37°C in the presence of 5 % CO_2 and were harvested at 80 - 90 % confluency. Each test compound (200 nl of 10 mM in 100 % v/v DMSO) was added to polystyrene 384 well cell culture microtitre plates (cat. no. 781073, 384 CellStar, Greiner Bio One, AT) using the Echo 550® Liquid Handler (Labcyte Inc., US). To harvest the cells, 1.5 ml of trypsin/EDTA (cat. no. L11-004, 0.5 mg/mL and 0.22 mg/mL respectively, PAA Laboratories GmbH, AT) was added per T175 flask and incubated at 37 °C in the presence of 5 % CO_2 for 2 minutes. Detached cells were then resuspended in pre-warmed media to a density of 0.2 x 10^6cells/mL. From this cell suspension, 20 µl was added per well of a 384 well microtitre plate thereby giving a final test compound concentration of 100 µM and 0.1 % v/v DMSO. After 48 hours of incubation at 37 °C in the presence of 5 % CO_2, 20 µl of CellTiter-Glo® reagent (cat. no. #G7571, Promega Inc., US) was added per well and the plate placed upon a linear shaker for 1 minute at room

temperature and further incubated at room temperature without shaking for 10 minutes. The luminescence readout was performed using the EnVision® Multilabel Reader 2103 (PerkinElmer Inc, US) with a 0.5 second read time per well. Each assay plate also contained 16 wells for the positive control (cells prepared by treatment with cisplatin: 200 nl of 300 mM stock solution in 100 % v/v DMSO giving a final concentration of 3 mM cisplatin). The 16 wells for the negative controls per assay plate were prepared by treatment of cells with DMSO only (200 nL).Each compound was tested in triplicate and the pIC50 value, Standard Deviation, Hill Slope, Minimum Signal and Maximum Signal for each dose-response curve were obtained using a 4-parameter logistic fit in the XE module of ActivityBase (IDBS).

Assessment of mitochondrial toxicity

The 786-O (renal carcinoma) cell line was used for mitochondrial toxicity screening. Cells were maintained using RPMI-1640 medium containing 2mM glutamine, 100 U/mL penicillin G, 100 mg/mL streptomycin and 10% FCS. Cells were counted and diluted to a concentration of 75,000 cells/mL and 20 µL of this suspension (1,500 cells/well) were added to CellCarrier™384-well TC plates (PerkinElmer Inc.) and incubated for 36 h at 37 °C and 5% CO_2.Compound dilutions were prepared using a 384-well PP pre-dilution plate (Greiner Bio-One) and 20 µL of the dilution were transferred to the 786-O cells. The Low Controls were Valinomycin (final concentration of 1 µM and 1% DMSO v/v in column 23) and the High Controls were 1% DMSO v/v in column 24. After 6h incubation at 37°C and 5% CO_2, 10 µL of a 200 nM solution of MitoTracker® Red CMXRos (final concentration 50 nM) in pre-warmed cell culture media (RPMI-1640 supplemented with 10 % FCS, 100 U/mL Penicillin and 100 µg/mL Streptomycin) was added to each well and the 786-O cells was incubated for an additional 45 min at 37 °C and 5% CO_2.MitoTracker® Red CMXRos uptake was measured using an Opera HCS system (PerkinElmer) and image analysis was performed using Columbus 2.4.0 (PerkinElmer). All screening experiments were performed for the compounds as 11-point dose-responses in triplicates. The raw data were processed using GraphPad Prism (GraphPad Software Inc.) with outliers in control wells eliminated according to the 3-sigma method. The dose-

response curves were analysed using 4 parameter sigmoidal fit to obtain plausible results in the case non-sigmoidal dose-response curves.

Aurora B kinase assay

The assay used was the ADP-Glo Kinase Enzyme System from PromegaCorp. The assay was performed in 384 well white low volume plate (Corning Inc. NY, USA, 3824). The control compound used was SU6656 (Calbiochem, Germany, 572635) at a final concentration of 1 µM in column 23 and DMSO in column 24 at the same concentration (vol/vol) as the SU6656 control and the compound area. DMSO concentration is tolerated up to 2% final (vol/vol). An enzyme mastermix containing of 1x buffer, 50 µM DTT and 17.5 ng/µl (35 µl/well) Aurora B [all reagents provided in the kit] is prepared. A substrate mastermix containing of 1x buffer, 36 µM APT and 7.5 ng/µl (15 ng/well) MBP protein as substrate [buffer, MBP provided in the Aurora B Kinase Enzyme System kit; ultrapure ATP provided in the ADP-Glo Kinase Assay kit] is prepared. 2 µl of the enzyme mastermix and 2 µl of the substrate mastermix are added to each well of a 384 low volume plate the plate is sealed using Thermowell sealing tape (Corning Inc. NY, USA) and incubated for 45 min at RT. The enzymatic reaction is stopped by adding 4 µl ADP-Glo reagent [provided in the ADP-Glo Kinase Assay kit] the plate is sealed again using Thermowell sealing tape (Corning Inc. NY, USA) and incubated for 40 min at RT. Afterwards 8 µl Detection Reagent are added to each well and the plate is sealed again The plate is incubated for 45 min at RT and afterwards luminescence is measured using the EnVision® Multilabel Reader 2103 (PerkinElmer Inc, US).Each compound was tested in triplicate and the pIC50 value, Standard Deviation, Hill Slope, Minimum Signal and Maximum Signal for each dose-response curve were obtained using a 4-parameter logistic fit in the XE module of ActivityBase (IDBS). All IC_{50} data were associated with < 10 % SD.

Solubility assays

UV-visible spectroscopy was used to measure the solubility of compound **2**. The experiments were carried out with the instrument CARY 50. Six different solutions (3.125, 6.25, 12.5, 25, 50 and 100 µM) were prepared. The maximum of absorbance was found at 334 nm and epsilon was calculated.

Four saturated solutions were prepared: 100 µM in water, 100 µM in PBS, 200 µM in PBS + 10 % DMSO and 10 mM in PBS + 50 % DMSO. The suspensions were left in incubation at 25°C for 18 hours, then filtered (0.2 µm). The absorbance at 334 nm was measured. One blank and three replicates of the same sample were performed for each solution. Using the calibration curve (Y = 0.0143x + 0.0033), we calculated the maximum solubility. Maximum solubility in water: 2.6 µM. Max solubility in PBS: 0.5 µM. Max solubility in PBS + 10 % DMSO = 85.5 µM. Max solubility in PBS + 50 % DMSO = 7.0 mM.

Compound 2 encapsulation in PLGA and solubilisation with cyclodextrins

The encapsulation of compound **2** on PLGA nanoparticles were obtained by a nanoprecipitation methodology. The polymer was dissolved in acetone at 20 mg/kg to for the diffusing phase. Then 0.5 mg of free compound were added for drug loading. This phase was then added to 10 ml of pluronic F127 (0.1 % in water) under moderate magnetic stirring at room temperature. For the evaporation of the organic solvent, the emulsion was stirred for 2 hours. The formed NPs were recovered and washed by centrifugation and stored in PBS at 4 ºC until use. Quantification of incorporated compound was done by the indirect method using absorption spectrophotometry. Standard curves for each compound were performed using 334 nm. The encapsulation efficiency was calculated as the ratio between the initial quantity of compound added to produce the NPs and the quantity of non-encapsulated compound present in the recovery and washing supernatants over the initial quantity of compound added to produce the NPs. Particles were characterized by Dynamic Light Scattering (DLS); the size, polydispersity index and zeta-potential were determined using a Zetasizer Nano ZS (Malvern Instruments, Malvern, UK) with a detection angle of 173°. Measurements were made in triplicate at 25 °C. Compound **2** was solubilised with hydroxypropyl-β-cyclodextrin (50% w/vol) /(Cavasol ® W7 HP Pharma, Ashland).

Pharmacokinetics of compound 2

Plasma samples from 6 BALB/c mice treated with compound **2** administered alone (1mg/kg IV) (5, 15 and 30 min post administration, p.a.), in PLGA nanoparticles (1m/kg/IV and oral) (0, 5, 15, 30, 45, 60 min and then 1, 3m 24, 48 and 72 hours p.a.) and solubilized with cyclodextrins (NMRI mice, 4 mg/kg/per os) (1, 6 and 24 hours p.a.) were analyzed by HPLC. Analysis was carried out with a modular Jasco HPLC fitted with a Hypersil BDS C18 column (250 x 4.6 mm, 5 μm) (Thermo Scientific) as stationary phase. Samples were treated with acetonitrile (ACN), vortexed, centrifuged (15 min, 6000 rpm), filtered through a 0.45 μm filter (Pall GHP Acrodisc GF) and assayed. Mobile phase was ACN:pure water (35:65), flow rate was 1.5 mL/min, injection loop was 100 μL and detection at a wavelength of 335 nm. Sulfate and glucuronide conjugation of compound **2** was tested.[58]

Ethics Statement

All experiments performed at IBMC were carried out in accordance with the IBMC.INEB Animal Ethics Committees and the Portuguese National Authorities for Animal Health guidelines, according to the statements on the directive 2010/63/EU of the European Parliament and of the Council.

The experimental design and housing conditions at UCM were approved by the Committee of Animal Experimentation (Universidad Complutense de Madrid) and regional authorities (Community of Madrid) (Ref. PROEX 169/15). Experiments were carried out at the animal house with official identification code ES280790001164 following the 3Rs principles. Animal handling and sampling were performed by trained and officially qualified personnel.

Supporting Information

- General structures of the flavonoids (Figure S1); code, chemical structure, purity and IC_{50} values of the 38 natural compounds screened (Table S1); X-ray crystallographic data (Table S2 and S3); inhibitory activity of the synthetic flavonols against *Tb*PTR1 and *Lm*PTR1 (Table S4); docking analysis (Table S5 and S6); sequence alignment of *Tb*PTR1 and *Lm*PTR1 (Figure

S2); inhibitory activity of the synthetic flavonols against hDHFR, *Tb*DHFR and *Lm*DHFR (Table S7); ADME-Tox data (Table S8); antiparasitic activity of the synthesized compounds alone (Table S9) and in combination with MTX and synergy coefficients (Table S10 and S11); isobologram and dose-effect curves for the combination of MTX and compound 13 (Figure S3); toxicity of the combination on THP-1 cells (Table S12); plasma concentration of compound 2 in BALB/c mice (Figure S4); nanoparticles characterization by Dynamic Light Scattering (Table S13), crystal structures used for conserved water analysis in *Tb*PTR1 and *Lm*PTR1 (Table S14 and S15); kinetic characterization of PTR1 and DHFR (Table S16); characterization of the compounds 1-16 and of the intermediates 17-24.

- PDB format files of the docking solutions for the synthesized flavonols.

- Molecular formula strings

PDB ID CODES

PDB code 5JCJ was used for docking of compounds **1-16** (TbPTR1). PDB code 1E92 was used for docking of compounds **1-16** (LmPTR1). The Protein Data Bank accession codes of the X-ray crystallographic structures of TbPTR1 in complex with **NP-13**, **NP-29**, **2** and **7** are 5JDC, 5JCX, 5JDI and 5JCJ, respectively. Authors will release the atomic coordinates and experimental data upon article publication.

Author Contributions

^ C.B., R.L., C.P., and I. P. contributed equally and are considered as co-first authors.

Corresponding Author

Prof. Maria Paola Costi phone, 0039-059-205-8579; E-mail, mariapaola.costi@unimore.it

Prof. Stefano Mangani phone,0039 0577 234255 - 4252E-mail, stefano.mangani@unisi.it

Dr. Stefania Ferrari phone, 0039-059-205-8578; E-mail, stefania.ferrari@unimore.it

ACKNOWLEDGEMENT

This project has received funding from the European Union's Seventh Framework Programme for research, technological development and demonstration under grant agreement n° 603240 (NMTrypI - New Medicine for Trypanosomatidic Infections). http://www.nmtrypi.eu/.

We acknowledge the European Synchrotron RadiationFacility (ESRF, Grenoble, France) and the Diamond Light Source (DLS, Didcot, United Kingdom)for providing synchrotron-radiation facilities and we would like to thank all of the staff for assistance in using the beamlines. The research leading to these results has received funding from the European Community's Seventh Framework Programme (FP7/2007-2013) under BioStruct-X (grant agreement N°283570). IP, SH and RCW gratefully acknowledge the support of the Klaus Tschira Foundation. We thank Zaheer-ul-HaqQasmifor his contributions to the initial computational analysis of the natural product library which were done with the support of the Alexander von Humboldt Foundation at HITS.

ABBREVIATIONS

WHO, World Health Organization; NTDs, Neglected Tropical diseases; HAT**,** Human African trypanosomiasis; DNDi, Drugs for Neglected Diseases initiative; DHFR, dihydrofolate reductase, *Tb*PTR1, *Trypanosoma brucei* pteridine reductase 1; *Lm*PTR1, *Leishmania major* pteridine reductase 1; MTX, methotrexate; *L. infantum*, *Leishmania infantum*; *L. donovani*, *Leishmania donovani*; *T. brucei, Trypanosoma brucei*; *T. cruzi, Trypanosoma cruzi*; $CDCl_3$, deuterated trichloromethane, EtOH, Ethanol; MeOH, Methanol; NaOH, sodium hydroxide; TMS, Trimethylsilane; DLS, dynamic light scattering; NPs, nanoparticles; PLGA, Poly(lactic-co-glycolicacid); IV, intravenous; PBS, phosphate-buffered saline; ACN, acetonitrile; FBS, fetal bovine serum; EC_{50}, half maximal effective concentration; CC_{50}, half maximal cytotoxicity concentration; THP1, human monocytic cell line; A549, human lung adenocarcinoma epithelial cell line; WI-38, foetal lung fibroblasts cell lines; DRC, dose-response curve.

REFERENCES

(1) Castillo, E.; Dea-Ayuela, M. A.; Bolás-Fernández, F.; Rangel, M.; González-Rosende, M.E. The kinetoplastid chemotherapy revisited: current drugs, recent advances and future perspectives. *Curr. Med. Chem.* **2010**, *17* (33), 4027-4051.

(2) Machado-Silva, A.; Guimarães, P. P.; Tavares, C. A.; Sinisterra, R. D. New perspectives for leishmaniasis chemotherapy over current anti-leishmanial drugs: a patent landscape. *Expert Opin. Ther. Pat.* **2015**, *25* (3), 247-260.

(3) Moraes, C. B.; Freitas-Junior, L. H.; Costantino, L.; Costi, M. P.; Coron, R. P.; Smith, T.; Siqueira-Neto, J. L.; Mckerrow, J.; Cordeiro-da-Silva, A. Current and Future Chemotherapy For Chagas Disease. *Curr. Med. Chem*. **2015**, *22* (37), 4293-4312.

(4) Barret, M. P.; Vincent, I. M.; Burchmore, R. J.; Kazibwe, A. J.; Matovu, E. Drug resistance in human African trypanosomiasis. *Future Microbiol*. **2011**, *6*, 1037-1047.

(5) Chakravarty, J.; Sundar, S. Drug resistance in Leishmaniasis. *J. Glob. Infect. Dis.* **2010**, *2*, 167-176.

(6) Chatelain, E.; Ioset, J. R. Drug discovery and development for neglected diseases: the DND*i* model. *Drug Des. Devel. Ther.* **2011**, *5*, 175–181.

(7) Gilbert, I. H. Drug discovery for neglected diseases: molecular target-based and phenotypic approaches. *J. Med. Chem.* **2013**, *56* (20), 7719-7726.

(8) Hyde, J. E. Exploring the folate pathway in Plasmodium falciparum. *Acta Trop.* **2005**, *94* (3), 191-206.

(9) Gilbert, I. H. Inhibitors of dihydrofolate reductase in Leishmania and trypanosomes. *Biochim. Biophys. Acta.* **2002**, *1587* (2-3), 249-257.

(10) Dawson, A.; Gibellini, F.; Sienkiewicz, N.; Tulloch, L. B.; Fyfe, P. K.; McLuskey, K.; Fairlamb, A. H.; Hunter, W. N. Structure and reactivity of Trypanosoma brucei pteridine reductase: inhibition by the archetypal antifolate methotrexate. *Mol. Microbiol.* **2006**, *61* (6), 1457-1468.

(11) Guerrieri, D.; Ferrari, S.; Costi, M. P.; Michels, P. A. Biochemical effects of riluzole on Leishmania parasites. *Exp. Parasitol.* **2013**, *133* (3), 250-254.

(12) Barrack, K. L.; Tulloch, L. B.; Burke, L. A.; Fyfe, P. K.; Hunter, W. N. Structure of recombinant Leishmania donovani pteridine reductase reveals a disordered active site. *Acta. Crystallogr. Sect. F Struct. Biol. Cryst. Commun.* **2011**, *67* (Pt 1), 33-37.

(13) Ferrari, S.; Morandi, F.; Motiejunas, D.; Nerini, E.; Henrich, S.; Luciani, R.; Venturelli, A.; Lazzari, S.; Calò, S.; Gupta, S.; Hannaert, V.; Michels, P. A.; Wade, R. C.; Costi, M. P. Virtual screening identification of non folate compounds, including a CNS drug, as antiparasitic agents inhibiting pteridine reductase. *J. Med. Chem.* **2011**, *54* (1), 211-221.

(14) Tulloch, L. B.; Martini, V. P.; Iulek, J.; Huggan, J. K.; Lee, J. H.; Gibson, C. L.; Smith, T. K.; Suckling, C. J.; Hunter, W. N. Structure-based design of pteridine reductase inhibitors targeting African sleeping sickness and the leishmaniases. *J. Med. Chem.* **2010**, *53* (1), 221-229.

(15) Cavazzuti, A.; Paglietti, G.; Hunter, W. N.; Gamarro, F.; Piras, S.; Loriga, M.; Allecca, S.; Corona, P.; McLuskey, K.; Tulloch, L.; Gibellini, F.; Ferrari, S.; Costi, M. P. Discovery of potent pteridine reductase inhibitors to guide antiparasite drug development. *PNAS.* **2008**, *105* (5), 1448-1453.

(16) Balunas, M. J.; Kinghorn, A. D. Drug discovery from medicinal plants. *Life Sci.* **2005**, *78* (5), 431-441.

(17) Annang, F.; Pérez-Moreno, G.; García-Hernández, R.; Cordon-Obras, C.; Martín, J.; Tormo, J. R.; Rodríguez, L.; de Pedro, N.; Gómez-Pérez, V.; Valente, M.; Reyes, F.; Genilloud, O.; Vicente, F.;

Castanys, S.; Ruiz-Pérez, L. M.; Navarro, M.; Gamarro, F.; González-Pacanowska, D. High-throughput screening platform for natural product-based drug discovery against 3 neglected tropical diseases: human African trypanosomiasis, leishmaniasis, and Chagas disease. *J. Biomol. Screen.* **2015**, *20* (1), 82-91.

(18) Harvey, A.L. Natural products in drug discovery. *Drug Discov. Today.* **2008**, *13* (19-20), 894-901.

(19) Harvey, A. L. The re-emergence of natural products for drug discovery in the genomics era. *Nature Reviews Drug Discovery.* **2015**, *14*, 111-129.

(20) Ndjonka, D.; Rapado, L. N.; Silber, A. M.; Liebau, E.; Wrenger, C. Natural Products as a Source for Treating Neglected Parasitic Diseases. *Int. J. Mol. Sci.* **2013**, *14*, 3395-3439.

(21) Singh, N.; Mishra, B. B.; Bajpai, S.; Singh, R. K.; Tiwari, V. K. Natural product based leads to fight against leishmaniasis. *Bioorg. Med. Chem*. **2014**, *22* (1), 18-45.

(22) Tasdemir, D.; Kaiser, M.; Brun, R.; Yardley, V.; Schmidt, T. J.; Tosun, F.; Rüedi, P. Antitrypanosomal and antileishmanial activities of flavonoids and their analogues: in vitro, in vivo, structure-activity relationship, and quantitative structure-activity relationship studies. *Antimicrob. Agents Chemother.* **2006**, *50* (4), 1352-1364.

(23) da Silva, E. R.; MaquiaveliCdo, C.; Magalhães, P. P. The leishmanicidal flavonols quercetin and quercitrin target Leishmania (Leishmania) amazonensis arginase. *Exp. Parasitol.* **2012**, *130* (3), 183-188.

(24) Manjolin, L. C.; dosReis, M. B.; MaquiaveliCdo, C.; Santos-Filho, O. A.; da Silva, E. R. Dietary flavonoids fisetin, luteolin and their derived compounds inhibit arginase, a central enzyme in Leishmania (Leishmania) amazonensis infection. *Food Chem.* **2013**, *141* (3), 2253-2262.

(25) Mamani-Matsuda, M.; Rambert, J.; Malvy, D.; Lejoly-Boisseau, H.; Daulouède, S.; Thiolat, D.; Coves, S.; Courtois, P.; Vincendeau, P.; Mossalayi, M. D. Quercetin induces apoptosis of Trypanosoma brucei gambiense and decreases the proinflammatory response of human macrophages. *Antimicrob. Agents Chemother.* **2004**, *48* (3), 924-929.

(26) Dias, T. A.; Duarte, C. L.; Lima, C. F.; Proença, M. F.; Pereira-Wilson, C. Superior anticancer activity of halogenated chalcones and flavonols over the natural flavonol quercetin. *Eur. J. Med. Chem.* **2013**, *65*, 500-510.

(27) Juvale, K.; Stefan, K.; Wiese M. Synthesis and biological evaluation of flavones and benzoflavones as inhibitors of BCRP/ABCG2. *Eur. J. Med. Chem.* **2013**, *67*, 115-126.

(28) Setzer, W. N; Ogungbe, I.V. In-silico Investigation of Antitrypanosomal Phytochemicals from Nigerian Medicinal Plants. *PLoS Negl. Trop. Dis*. **2012**, *6* (7), e1727.

(29) Kavanagh, K. L.; Jornvall, H.; Persson, B.; Oppermann, U. Medium- and short-chain dehydrogenase/reductase gene and protein families : the SDR superfamily: functional and structural diversity within a family of metabolic and regulatory enzymes. *Cell. Mol. Life Sci.* **2008**, *65*, 3895-3906.

(30) Gourley, D. G.; Schuttelkopf, A. W.; Leonard, G. A.; Luba, J.; Hardy, L. W.; Beverley, S. M.; Hunter, W. N. Pteridine reductase mechanism correlates pterin metabolism with drug resistance in trypanosomatid parasites. *Nat. Struct. Biol.* **2001**, *8*, 521-525.

(31) Dawson, A.; Gibellini, F.; Sienkiewicz, N.; Tulloch, L. B.; Fyfe, P. K.; McLuskey, K.; Fairlamb, A. H.; Hunter, W. N. Structure and reactivity of Trypanosoma brucei pteridine reductase: inhibition by the archetypal antifolate methotrexate. *Mol. Microbiol.* **2006**, *61* (6), 1457-1468.

(32) Chatelain, E. Chagas disease drug discovery: toward a new era. *J. Biomol. Screen.* **2015**, *20* (1), 22-35.

(33) Katsuno, K.; Burrows, J. N.; Duncan, K.; Hooft van Huijsduijnen, R.; Kaneko, T.; Kita, K.; Mowbray, C. E.; Schmatz, D.; Warner, P.; Slingsby, B. T. Hit and lead criteria in drug discovery for infectious diseases of the developing world. *Nat. Rev. Drug Discov.* **2015**, *14* (11), 751-758.

(34) Chou, T. C. Theoretical basis, experimental design, and computerized simulation of synergism and antagonism in drug combination studies. *Pharmacol. Rev.* **2006**, *58* (3), 621-681.

(35) Jones, G.; Willett, P.; Glen, R. C. Molecular recognition of receptor sites using a genetic algorithm with a description of desolvation. *J. Mol. Biol*. **1995**, *245*, 43–53.

(36) Jones, G.; Willett, P.; Glen, R. C.; Leach, A. R.; Taylor, R. Development and validation of a genetic algorithm for flexible docking. *J. Mol. Biol*. **1997**, *267*, 727–748.

(37) Schrödinger Release 2015-4: Maestro, version 10.4, Schrödinger, LLC, New York, NY, 2015.

(38) Sanschagrin, P. C.; Kuhn, L.A. Cluster Analysis of Consensus Water Sites in Thrombin and Trypsin Shows Conservation Between Serine Proteases and Contributions to Ligand Specificity. *Prot. Sci.* **1998**, *7*, 2054-2064.

(39) Small-Molecule Drug Discovery Suite 2015-4: Glide, version 6.9, Schrödinger, LLC, New York, NY, 2015.

(40) Friesner, R. A.; Murphy, R. B.; Repasky, M. P.; Frye, L. L.; Greenwood, J. R.; Halgren, T. A.; Sanschagrin, P. C.; Mainz, D. T. Extra Precision Glide: Docking and Scoring Incorporating a Model of Hydrophobic Enclosure for Protein-Ligand Complexes. *J. Med. Chem.* **2006**, *49*, 6177-6196.

(41) Halgren, T. A.; Murphy, R. B.; Friesner, R. A.; Beard, H. S.; Frye, L. L.; Pollard, W. T.; Banks, J. L. Glide: A New Approach for Rapid, Accurate Docking and Scoring. 2. Enrichment Factors in Database Screening. *J. Med. Chem.* **2004**, *47*, 1750-1759.

(42) Friesner, R. A.; Banks, J. L.; Murphy, R. B.; Halgren, T. A.; Klicic, J. J.; Mainz, D. T.; Repasky, M. P.; Knoll, E. H.; Shaw, D. E.; Shelley, M.; Perry, J. K.; Francis, P.; Shenkin, P. S. Glide: A New Approach for Rapid, Accurate Docking and Scoring. 1. Method and Assessment of Docking Accuracy. *J. Med. Chem.* **2004**, *47*, 1739-1749.

(43) Li, H.; Robertson, A.D.; Jensen, J.H. Very Fast Empirical Prediction and Interpretation of Protein pKa Values. *Proteins.* **2005**, *61*, 704-721.

(44) Cardinale, D.; Guaitoli, G.; Tondi, D.; Luciani, R.; Henrich, S.; Salo-Ahen, O.M.H.; Ferrari, S.; Marverti, G.; Guerrieri, D.; Ligabue, A.; Frassineti, C.; Pozzi, C.; Mangani, S.; Fessas, D.; Guerrini, R.; Ponterini, G.; Wade, R.C.; Costi, M.P. Protein-protein interface-binding peptides inhibit the cancer therapy target human thymidylate synthase. *PNAS.* **2011**, *108*, E542-E549.

(45) Benvenuti, M.; Mangani, S. Crystallization of soluble proteins in vapor diffusion for x-ray crystallography. *Nat. Protoc.* **2007**, *2* (7), 1633-1651.

(46) Leslie, A. G. The integration of macromolecular diffraction data. *ActaCrystallogr. D Biol. Crystallogr.* **1999**, *62*, 48-57.

(47) Evans P. Scaling and assessment of data quality. *ActaCrystallogr. D Biol. Crystallogr.* **2006**, *62*, 72-82.

(48) Collaborative Computational Project, Number 4. The CCP4 suite: programs for protein crystallography. *ActaCrystallogr. D Biol. Crystallogr*. **1994**, *50*, 760-763.

(49) Vagin, A.; Teplyakov, A. MOLREP: an automated program for molecular replacement. *J. Appl. Crystallogr.* **1997**, *30*, 1022-1025.

(50) Dawson, A.; Tulloch, L. B.; Barrack, K. L.; Hunter, W. N. High-resolution structures of Trypanosoma brucei pteridine reductase ligand complexes inform on the placement of new molecular entities in the active site of a potential drug target. *ActaCrystallogr. D. Biol. Crystallogr.* **2010**, *66*, 1334-1340.

(51) Murshudov, G. N.; Vagin, A.; Dodson, E. J. Refinement of macromolecular structures by themaximum-likelihood method. *ActaCrystallogr. D Biol. Crystallogr.* **1997**, *53*, 240-255.

(52) Emsley, P.; Cowtan, K. Coot: model-building tools for molecular graphics. *ActaCrystallogr. DBiol. Crystallogr.* **2004**, *60*, 2126-2132.

(53) Laskowski, R. A.; MacArthur, M. W.; Moss, D. S.; Thornton, J. M.PROCHECK - a program to check the stereochemical quality of protein structures. *J. Appl. Crystallogr.* **1993**, *26*, 283-291.

(54) McNicholas, S.; Potterton, E.; Wilson, K. S.; Noble M. E. M. Presenting your structures: the CCP4mg molecular-graphics software. *ActaCrystallogr. D. Biol. Crystallogr.* **2011**, *67*, 386-394.

(55) Shanks, E. J.; Ong, H. B.; Robinson, D. A.; Thompson, S.; Sienkiewicz, N.; Fairlamb, A. H.; Frearson, J. A. Development and validation of a cytochrome c-coupled assay for pteridine reductase 1 and dihydrofolate reductase. *Anal. Biochem.* **2010**, *396* (2), 194-203.

(56) Sereno, D.; Cavaleyra, M.; Zemzoumi, K.; Maquaire, S.; Ouaissi, A.; Lemesre, J. L. Axenically grown amastigotes of Leishmania infantum used as an in vitro model to investigate the pentavalent antimony mode of action. *Antimicrob. Agents Chemother.* **1998**, *42* (12), 3097-3102.

(57) Bowling, T.; Mercer, L.; Don, R.; Jacobs, R.; Nare, B. Application of a resazurin-based high-throughput screening assay for the identification and progression of new treatments for human African trypanosomiasis. *Int. J. Parasitol. Drugs Resist*. **2012**, *2*, 262-270.

(58) Shia, C.; Tsai, S.; Kuo, S.; Hou, Y.; Chao, P. L. Metabolism and pharmacokinetics of 3,3‘,4‘,7-tetrahydeoxyflavone (fisetin), 5-hydroxyflavone and 7-hydroxyflavone and antihemolysis effects of fisetin and its serum metabolites. *J. Agric. Food Chem.* **2009**, *57*, 83-89.

Figure Legends

Figure 1. Activity profile of the 38 phytochemicals screened against*Tb*PTR1, hTS and hDHFR and against the *T. brucei* parasite. The IC_{50} is indicated by the color : dark green -0-30 μM; green - 31-90 μM; light green - 90-150 μM; yellow - 151-250 μM; red -> 250 μM; gray, not tested. * Catechins; ** Triterpenes; ***Antraquinones.

Figure 2. Crystal structures of *Tb*PTR1 (gray cartoon, interacting residues in sticks) in complex with NADPH/$NADP^+$(in sticks, black carbon atoms) and four inhibitors (in sticks) **A) NP-29** (cyan), **B) NP-13** (orange), **C)** compound **2** (lilac), and **D)** compound **7** (yellow). Hydrogen bond interactions (dashed lines) in the active site are shown. The 2Fo-Fc electron density maps corresponding to the inhibitors (dark blue wire) andNADPH/$NADP^+$(light blue wire), contoured at the1σ level are shown. The chemical structures and atom names of the ligands are specified in the insets.

Figure 3. Design of the synthetic library (left). NP-13 (in yellow) into *Tb*PTR1 (in gray). The amino acids involved in the interactions of the designed compounds are shown in different colored. For clarity reasons, two residues involved in the interactions are not shown (Cys 168 and Asn 175). Superimposition of the four crystal structures of *Tb*PTR1 (right) (chain A gray ribbon; chain D pink ribbon; relevant active site residues as light blue sticks) in complex with NADPH/$NADP^+$ (sticks, black carbon atoms) and the inhibitors (stick) **NP-13** (cyan), **NP-29** (coral), compound **2** (lilac), compound **7** (yellow). The three different binding modes adopted by the ligands can be appreciated as well as the movement of Trp221 (yellow sticks) upon binding of compound **7**.

Figure 4. Inhibitory activity against *Tb*PTR1 (in gray) and *Lm*PTR1 (in black). The control compound was pyrimethamine, a PTR1 inhibitor (100% inhibition at 50 μM against both PTR1 enzymes).

Figure 5. Comparison of the effects of hydroxyl substituents at the R6 (left) and the R7 (right) positions of Ring A on the binding of the synthetic flavonoids to *Tb*PTR1. Superimposition of constraint docking poses for compound **2** (in sticks, lilac carbons) and compound **5** (in sticks, pale green carbons) (left) and compound **3** (in sticks, orange carbons) and compound **6** (in sticks, brown carbons) (right) in *Tb*PTR1 (in cartoon with interacting residues in sticks with grey carbons) in complex with NADPH/$NADP^+$ (in sticks, black carbon atoms). A conserved water molecule is shown in ball-and-stick representation. Hydrogen bonds are indicated by dark gray dotted lines.

Figure 6. Comparison of the effects of hydroxyl and methoxy substituents at the R6 (left) and the R3' (left and right) positions on the binding of the synthetic flavonoids to *Tb*PTR1. Constraint docking poses are shown for compound **2** (in sticks, lilac carbons) and compound **10** (in sticks, dark green carbons) (left) and compound **9** (in sticks, pale cyan carbons) and compound **1** (in sticks, magenta carbons) (right) in *Tb*PTR1 (in cartoon with interacting residues in sticks with grey carbons) in complex with NADPH/$NADP^+$(in sticks, black carbon atoms). A conserved water molecule is shown in ball-and-stick representation. Hydrogen bonds are indicated by dark gray dotted lines. **Figure 7.** Superimposition of the crystal structure of *Lm*PTR1 (PDB ID 1E92, in cartoon representation and interacting residues in sticks representation. Chain A and D (containing Arg287) are colored in pale pink and magenta, respectively) and the best predicted receptor conformation obtained in the induced-fit docking study starting from this crystal structure (His241 in H-bonding contact to compound **7**) in complex with NADPH/$NADP^+$ (in sticks, black carbons) and compound **7** (in sticks, yellow carbons). A conserved water molecule is shown in ball-and-stick representation. Hydrogen bonds are indicated by dark gray dotted lines.

Figure 8. Early toxicity properties combined with inhibitory activity against *T. brucei*. The data are reported as a traffic light system. An ideal compound (I. comp.) should have all the parameters green. The cells are colored in green when the percentage of inhibition of *T. brucei* and the percentage of A549 and W1-38 cell growth is between 60 and 100, while the percentage of inhibition of CYP isoforms, hERG, Aurora B kinase and mitochondrial toxicity is between 0 and 30. Cells are colored in red when data indicates toxicity or inactivity. Yellow stands for a borderline value (30-60%): moderately active or slightly toxic compound.

Figure 9. Anti-parasitic activity of the synthesized compounds against *Trypanosoma brucei*(in gray), *Trypanosoma cruzi* (in green) and *Leishmania infantum* (in black) at 10 μM. The reference compounds were pentamidine (IC_{50} = 1.55 ± 0.24 nM) for *T. brucei*; miltefosine (IC_{50} = 2.65 ± 0.4 μM) for *L. infantum*; and nifurtimox (IC_{50} = 2.2± 0.4μM) for *T. cruzi*.

Figure 10. Trypanocidal activity of 8 synthesized compounds alone and in combination with MTX. The compounds were tested at three different concentration: 5 μM (in green), 2.5 μM (in light pink), 1.25 μM (in light blue).

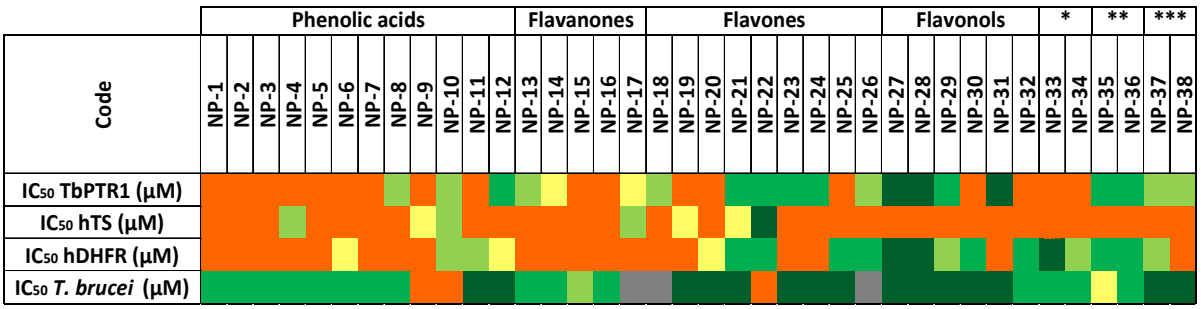
Phenolic acids
Flavanones
Flavones
Flavonols
*
**
***
Code
NP-1 NP-2 NP-3 NP-4 NP-5 NP-6 NP-7 NP-8 NP-9 NP-10 NP-11 NP-12 NP-13 NP-14 NP-15 NP-16 NP-17 NP-18 NP-19 NP-20 NP-21 NP-22 NP-23 NP-24 NP-25 NP-26 NP-27 NP-28 NP-29 NP-30 NP-31 NP-32 NP-33 NP-34 NP-35 NP-36 NP-37 NP-38
IC50 TbPTR1 (μM)
IC50 hTS (μM)
IC50 hDHFR (μM)
IC50 T. brucei (μM)

Figure 1

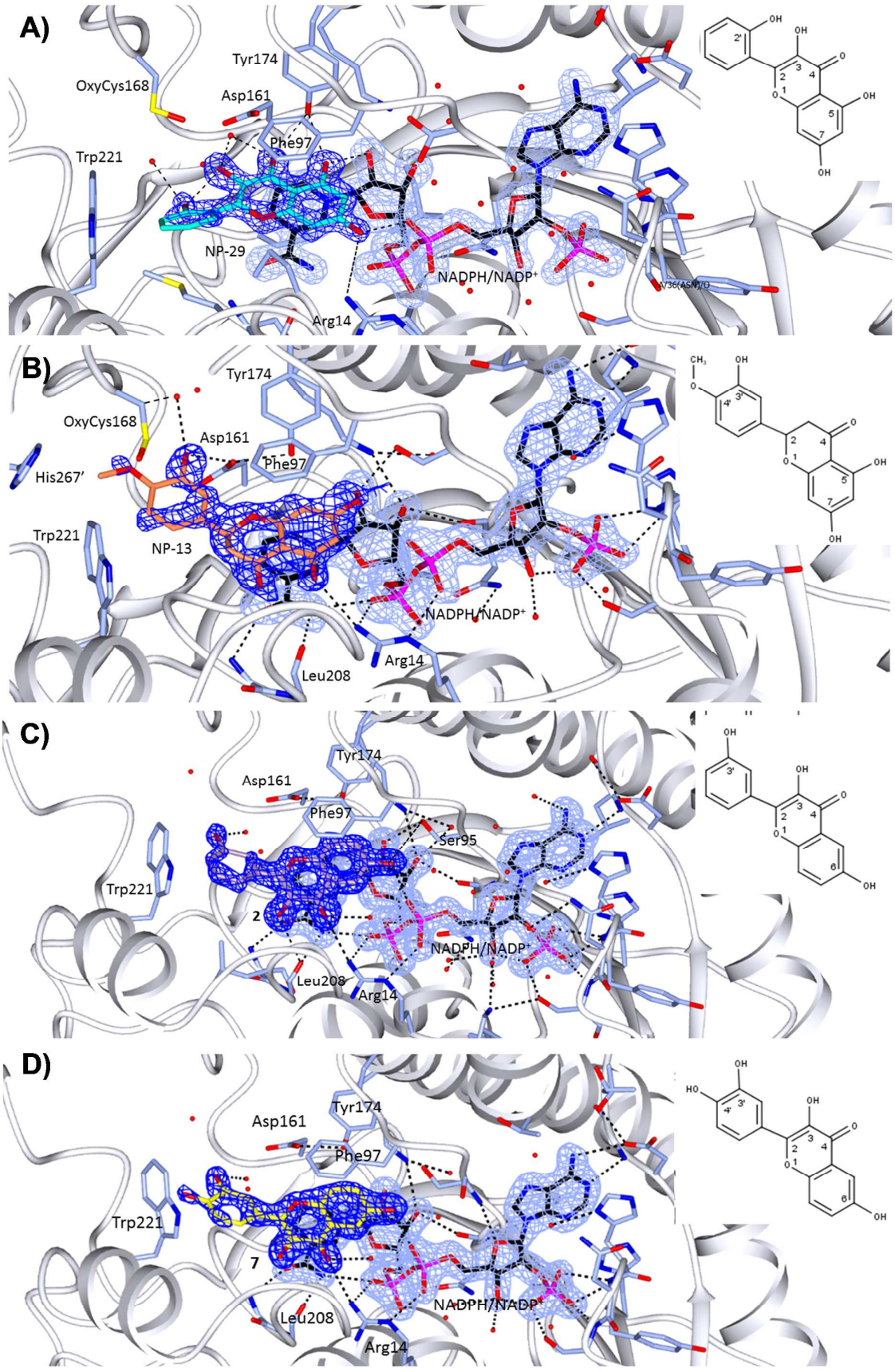
A)
Tyr174
OxyCys168
Asp161
Phe97
Trp221
NP-29
NADPH/NADP+
Arg14
B)
Tyr174
OxyCys168
Asp161
Phe97
His267'
Trp221
NP-13
NADPH/NADP+
Arg14
Leu208
C)
Tyr174
Asp161
Phe97
Ser95
Trp221
NADPH/NADP+
Leu208
Arg14
D)
Asp161
Tyr174
Phe97
Trp221
NADPH/NADP+
Leu208
Arg14

Figure 2.

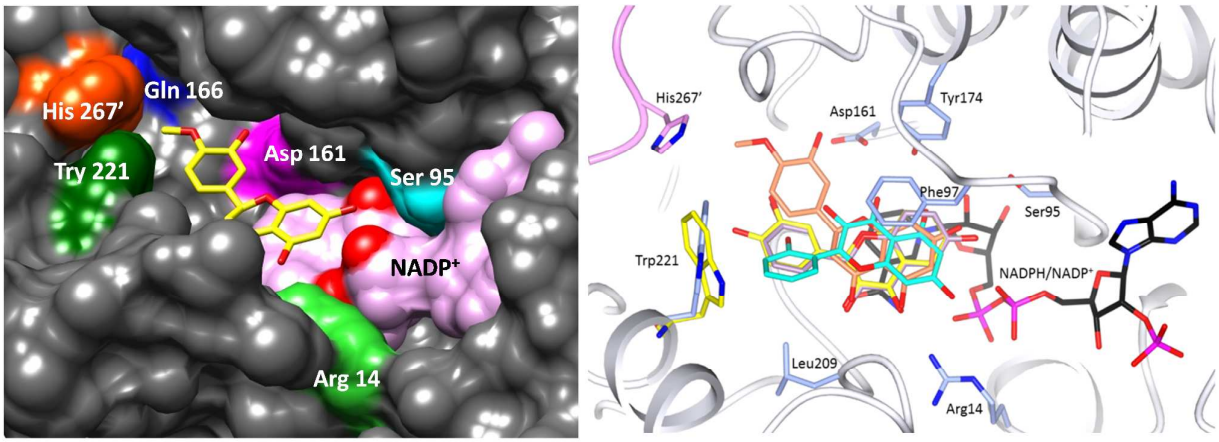
Gln 166
His 267'
Asp 161
Try 221
Ser 95
NADP+
Arg 14
His267'
Asp161
Tyr174
Phe97
Ser95
Trp221
NADPH/NADP+
Leu209
Arg14

Figure 3.

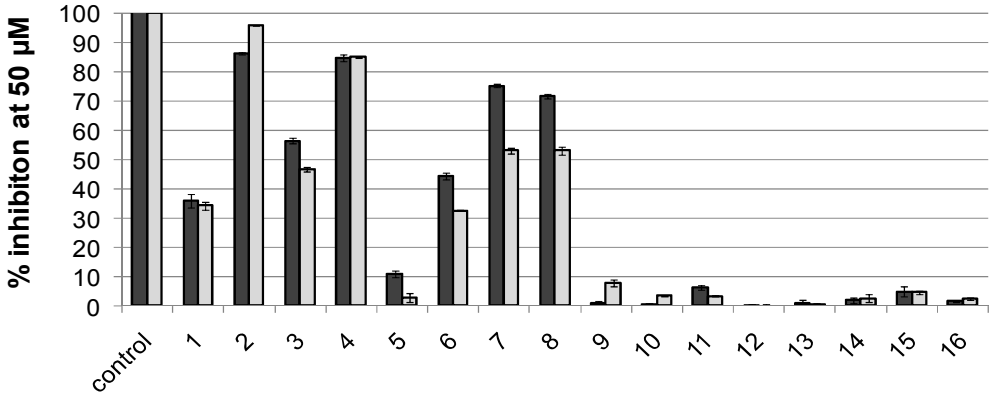
% inhibiton at 50 µM
100
90
80
70
60
50
40
30
20
10
0
control
1
2
3
4
5
6
7
8
9
10
11
12
13
14
15
16

Figure 4.

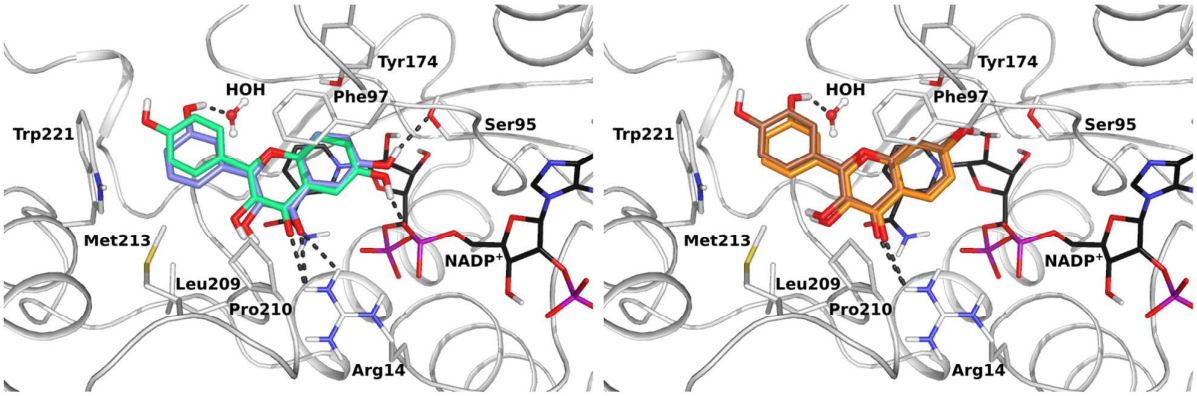
Tyr174
HOH
Phe97
Ser95
Trp221
Met213
NADP+
Leu209
Pro210
Arg14
Tyr174
HOH
Phe97
Ser95
Trp221
Met213
NADP+
Leu209
Pro210
Arg14

Figure 5.

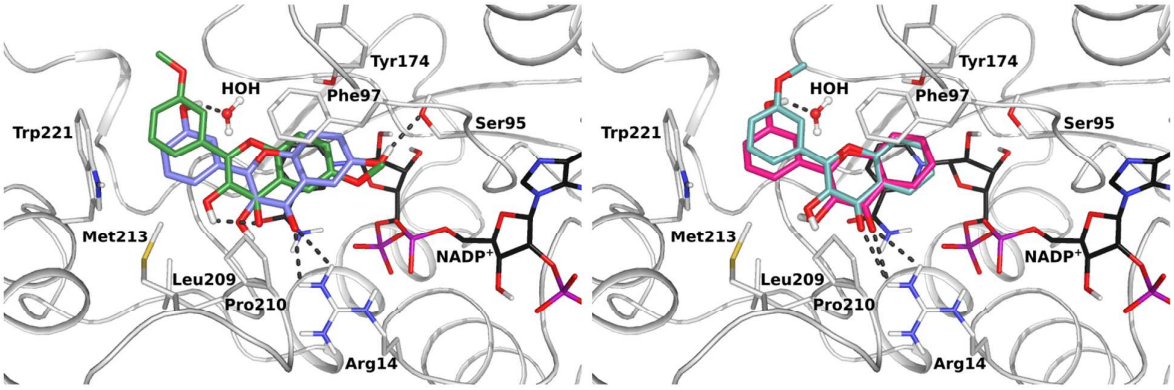
Tyr174
HOH
Phe97
Ser95
Trp221
Met213
NADP+
Leu209
Pro210
Arg14
Tyr174
HOH
Phe97
Ser95
Trp221
Met213
NADP+
Leu209
Pro210
Arg14

Figure 6.

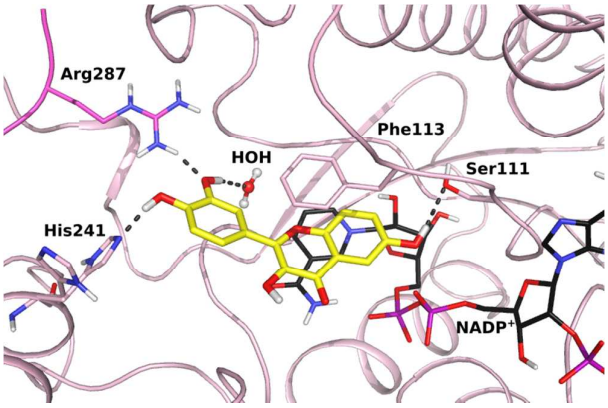

Figure 7.

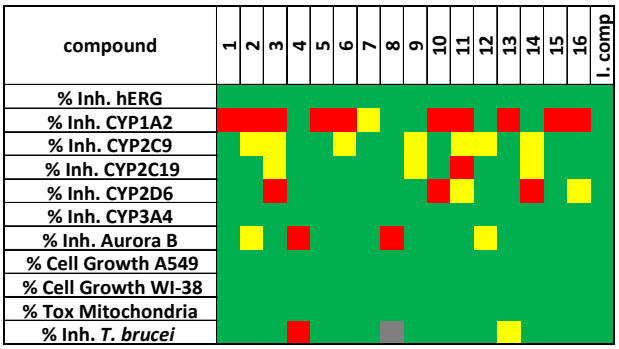
compound
1
2
3
4
5
6
7
8
9
10
11
12
13
14
15
16
l. comp
% Inh. hERG
% Inh. CYP1A2
% Inh. CYP2C9
% Inh. CYP2C19
% Inh. CYP2D6
% Inh. CYP3A4
% Inh. Aurora B
% Cell Growth A549
% Cell Growth WI-38
% Tox Mitochondria
% Inh. T. brucei

Figure 8.

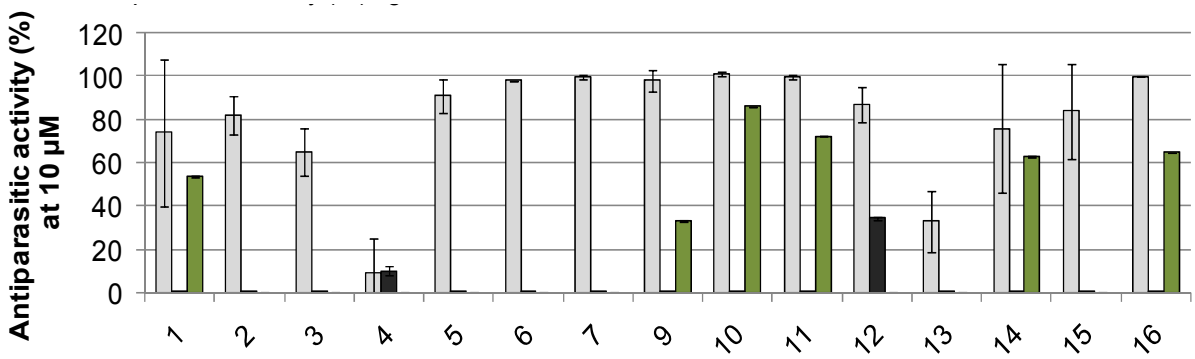
Antiparasitic activity (%) at 10 µM
120
100
80
60
40
20
0
1
2
3
4
5
6
7
9
10
11
12
13
14
15
16

Figure 9.

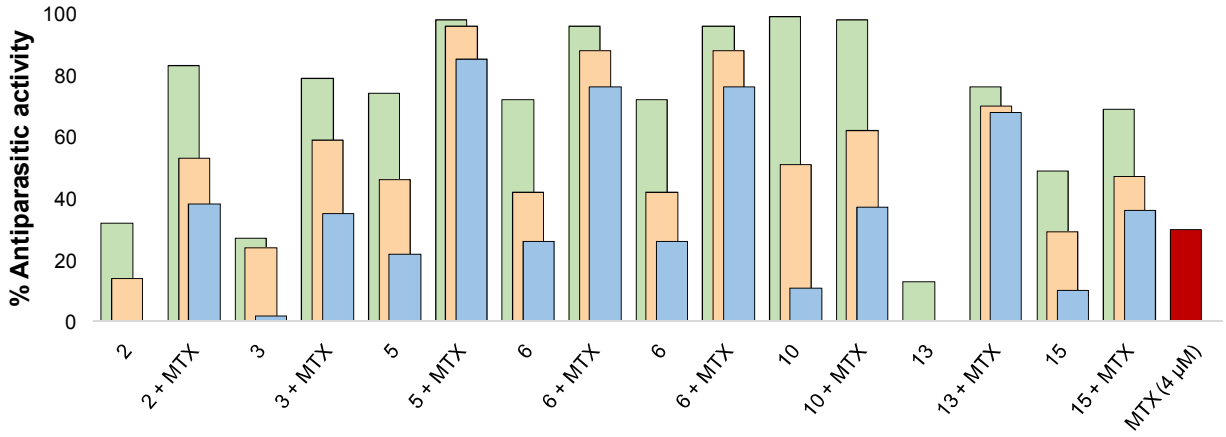
% Antiparasitic activity
100
80
60
40
20
0
2
2 + MTX
3
3 + MTX
5
5 + MTX
6
6 + MTX
6
6 + MTX
10
10 + MTX
13
13 + MTX
15
15 + MTX
MTX (4 µM)

Figure 10.

Table 1. Chemical structures and IC_{50} values for selected compounds from the screened natural products library.

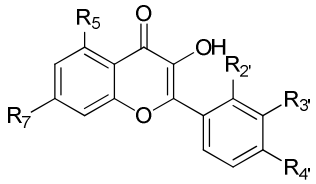

Comp.	R_5	R_7	$R_{2'}$	$R_{3'}$	$R_{4'}$	IC_{50} *Tb*PTR1 (μM)	IC_{50} *T. brucei* (μM)
NP-27	H	H	H	H	H	12,8	9,1
NP-28	OH	OH	H	H	OH	28,0	9,0
NP-29	OH	OH	OH	H	H	76,9	27,0
NP-31	OH	OH	H	OCH_3	OH	13,9	11,2

Table 2. EC_{50} against *T. brucei*, NOAEL and selectivity index of the synthesized compounds. EC_{50} and NOAEL represent the arithmetic average of at least two independent determinations done in triplicate.

Comp.	EC_{50} *T. brucei* (μM)	CC_{50} ± SD or NOAEL	Selectivity index (CC_{50}/EC_{50})
1	5.18±1.10	20	4
2	7.56±0.51	53±2	7
3	12.29±2.82	80±2	6
4	18.04±0.50	100	5
5	2.32±0.42	20	7
6	4.29±0.71	20	4
7	1.36±0.57	10	6
9	2.32±1.01	10	4
10	1.43±0.42	10	7
11	1.14±0.24	10	8
12	1.17±1.07	20	17
13	20.12±2.27	20	1
14	1.10±0.47	10	9
15	2.02±0.51	10	5
16	2.99±1.86	25	8
Pentamidine	0.00155±0.00024	10	6440

Table 3. Summary report of computer-simulated CI and DRI values for MTX and compound 13 combinations at 50%, 75%, 90% and 95% inhibition of *T. brucei* growth. Data reported are the average of three independent experiments. Data analysis was carried out using the CompuSyn software.[34]

Drug combination	Combination ratio	CI values at the reported EC				DRI values at the reported EC			
		EC_{50}	EC_{75}	EC_{90}	EC_{95}	EC_{50}	EC_{75}	EC_{90}	EC_{95}
MTX + compound 13	(2:1.5)	0.174 ± 0.047	0.075 ± 0.036	0.034 ± 0.023	0.020 ± 0.016	14.58 ± 3.71*	41.95 ± 10.52*	127.36 ± 60.20*	278.17 ± 172.13*
						11.72 ± 2.79*	27.45 ± 6.90*	65.56 ± 16.42*	119.72 ± 29.15*

*Values on top are for the MTX and on the bottom are for compound 13

Table 4. The *in vitro* activity against *T. brucei* of compound **2** in three different formulations. EC_{50} and NOAEL are the arithmetic mean of at least two independent determinations done in triplicate.

Preparation	*T. brucei* EC_{50} (µM)	THP1 CC_{50} ± SD or NOAEL
Compound 2	7.56 ± 0.51	53±2
PLGA-2	5.70 ± 0.23	>100
Cyclodextrin-2	3.27 ± 0.16	>100

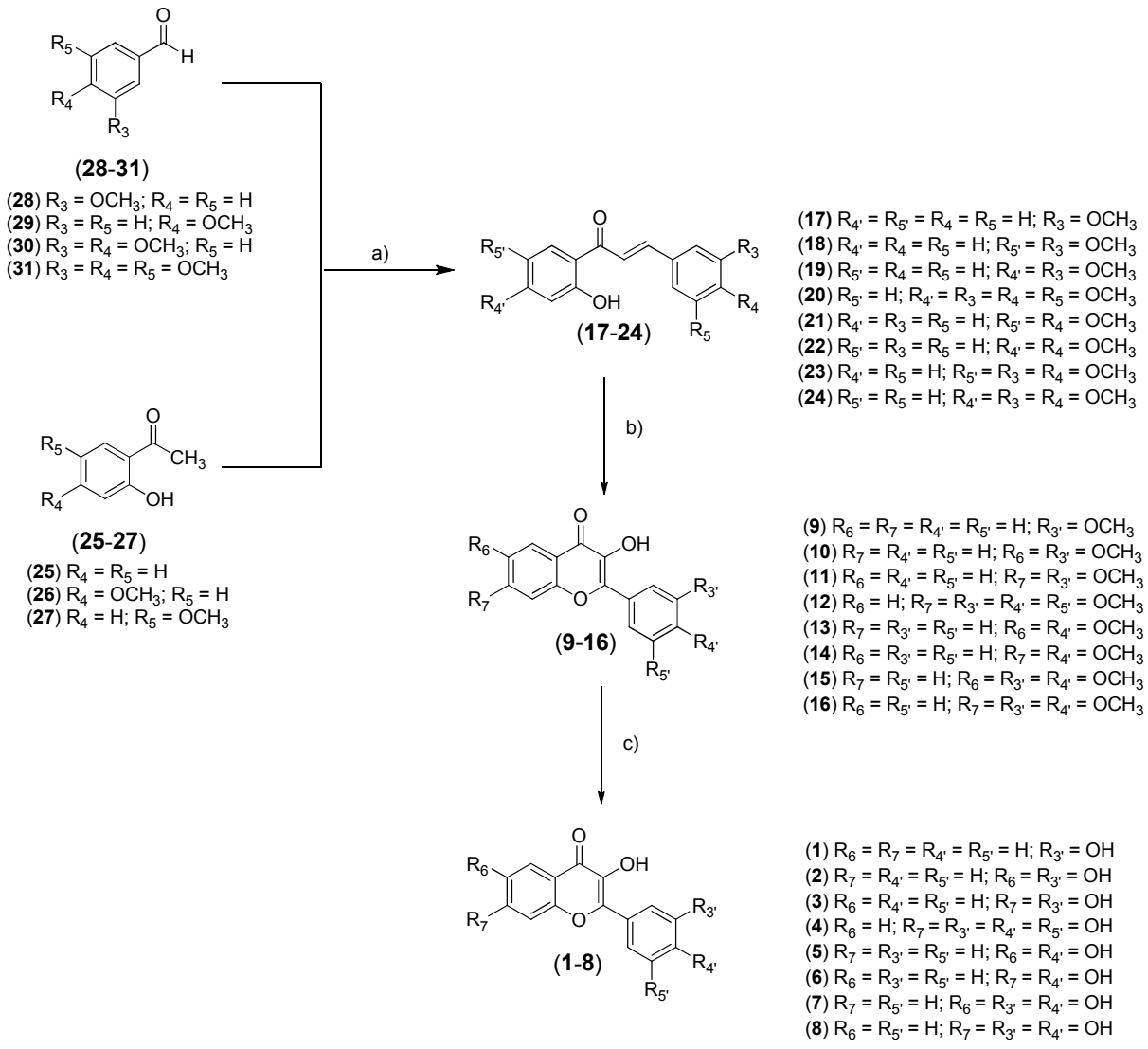

Scheme 1. Synthesis of the flavonols **1**-**16**. Reaction conditions: a) NaOH (3 M), EtOH, r.t. b) H_2O_2,NaOH (1 M), EtOH, r.t. c) BBr_3 (1 M in dry DMC), dry DMC, 0 °C → r.t.

TOC – Graphical Abstract